Correlation of Liver Injury and Biomechanical Predictors: A Study of Lateral and Oblique Impacts to Post-Mortem Human Subjects

Thesis

Presented in Partial Fulfillment of the Requirements for the Degree Master of Science in the Graduate School of The Ohio State University

By

Hannah Marie Gustafson, B.S.

Graduate Program in Mechanical Engineering

The Ohio State University

2009

Thesis Committee:

John H. Bolte IV, Advisor

Rebecca B. Dupaix

ABSTRACT

Research has shown that abdominal injuries account for 3-5% of injuries from motor vehicle crashes. However, abdominal injuries, especially to the solid organs of the abdomen such as the liver, represent a higher proportion of serious injuries. Previous work has shown a correlation between vascular pressure and liver injury in human surrogates and in pressurized *ex vivo* human and porcine livers when subjected to blunt impact. The objectives of this work are to further investigate the relationship between pressure and liver injury using post-mortem human surrogates. Specifically, the goals were to (1) conduct rigid impacts on PMHS (n=6) with re-pressurized abdominal vascular systems and measure vascular pressure; (2) determine if a correlation exists between measured vascular pressure and liver injury; (3) compare the results with previously proposed biomechanical predictors of abdominal injury.

For the study, each PMHS was instrumented with pressure sensors in the abdominal vessels, including the abdominal aorta, the hepatic veins, and the inferior vena cava. The subject's abdominal vessels were pressurized to physiological pressures using saline. For lateral impacts, the impact was applied to the right side of the subject. For oblique impacts, the impact was applied on the right side at 30 degrees anterior of lateral. The impact face was 30 cm by 15 cm. The lower edge of the impactor was aligned with the lowest rib at the mid-axillary line, typically rib eleven.

The injuries observed to the liver were similar to those documented in the Crash Injury Research Engineering Network (CIREN) trauma database and included three livers with superficial lacerations to the capsule and one liver injury with a serious burst injury. Using binary logistic regression to predict the injury risk, various pressure related variables had statistically significant relationships to injury including peak change in pressure (P_{max}), peak rate of change of pressure ($\dot{P}_{max}$) as well as $P_{max}\dot{P}_{max}$ and $[P(t)* \dot{P}(t)]_{max}$. The most statistically significant model related the peak rate of change of pressure to serious abdominal injury. This variable was also strongly correlated to the kinetic analog of the viscous criterion which was found as the peak of the rate of change of force times the compression ($[\dot{F} C]_{max}$). This suggests that the rate of change of pressure, similar to the kinetic analog of the viscous criterion, is a measurement of how quickly and how directly the liver is loaded. These results imply that pressure relates to injury and this could be used in an anthropomorphic test device (ATD) to predict abdominal injury. However, simply using a homogenous fluid filled insert for the abdomen may not be sufficient to determine if an organ would be injured or if it would move out of the way when impacted.

ACKNOWLEDGEMENT

I would like to acknowledge all those who have helped me along my way through this project. It is humbling to think of where I would be without the help and support of so many people.

First, I would like to thank Dr. John Bolte for his mentorship over the past two years. I am grateful for the experiences I have had in the Injury Biomechanics Research Laboratory (IBRL) and especially to John for providing advice and assistance in every aspect of this project.

Testing would not have been possible without the support of everyone in the IBRL including Mandy Agnew, Bridget Biteman, Kyle Icke, Yun Seok Kang, Matt Long, Austin Meek, Jason Miller, Brian Suntay, and Tony Vergis. Thank you to all of you for the times you stayed late to help with BMD or CT scans, set up cameras or instrumentation, or gave up your day to help test or do autopsy.

I would like to thank Dr. Steffen Sammet and Dr. John Landoll for being willing to do scans for us, even on short notice. I am also grateful to Mark and Michelle Whitmer for their assistance in preparing the subjects for testing. Mark and Michelle made our jobs so much easier and never failed to be cheerful while doing so.

Many thanks to Rod Herriott for his skills and knowledge that made test days go much smoother than it would have without him. Rod was ready to go on tests days with a pot of

coffee made when we got to the lab the morning and the willingness to do what needed to be done.

I would like to also thank Jason Stammen, Dan Rhule, and Dr. Bruce Donnelly at VRTC for their assistance on test days and analyzing the data. I appreciated all the ideas and suggestions for improving the experimental procedure and data analysis. Finally, deserving of special thanks is Dr. Rebecca Dupaix for serving on my committee and also for being a role model.

VITA

Hannah Marie Gustafson

May 1984……………………………………………Born- Cleveland, Ohio

June 2007…………………………………………....Bachelors of Science

The Ohio State University

September 2007 to August 2008……..……………….. Graduate Fellow

The Ohio State University

September 2008 to present………………………………Graduate Research Associate

The Ohio State University

Major Field: Mechanical Engineering

TABLE OF CONTENTS

LIST OF FIGURES

LIST OF TABLES

Chapter 1: Introduction

1.1 Motivation

Abdominal injuries are important to study because they occur commonly and tend to be more life threatening than injuries to other regions of the body. Ricci (1980) investigated data from the National Crash Severity Study (NCSS) from January 1977 to March 1979. The NCSS database required that the most severe injury occurred to an occupant of a towed vehicle. Injuries to the occupants were coded using the Abbreviated Injury Scale (AIS) ratings. AIS ratings range from 1 for a minor injury to 6 for injuries from which death is likely. Ricci found that injuries to the abdomen represented 3.8% of all injuries. However, the abdomen injuries represented a higher proportion of serious injuries. Injuries to the abdomen represented 8.3% of Abbreviated Injury Scale (AIS) 3+ injuries, 29.9% of AIS 4+, and 30.7% of AIS 5+. Similarly, Rouhana and Foster (1985) analyzed the NCSS dataset looking specifically at side impacts where the vehicle sustained damage to the right or left side of the vehicle. In this analysis, it was found that abdominal injuries represented 15.6 % of AIS 3+ injuries, 24.2% of AIS 4+ injuries and 21% of AIS 5+ injuries.

Elhagediab and Rouhana (1998) analyzed the National Automotive Sampling System (NASS) database from 1988 to 1994, including cars and light trucks involved in fontal impacts without rollover. It was found that abdominal injuries comprised 8% of the AIS 3+ injuries but represented 16.5% of AIS 4+ injuries and 20.5% of AIS 5+ injuries. Lee and Yang (2002) reported that abdominal injuries constituted 5.2% of all injuries but 15.6% of Abbreviated Injury Scale

1

(AIS) 3+ injuries in the National Automotive Sampling System (NASS) database for the years 1993 through 1997. These studies revealed that increasing frequency of abdominal injuries when considering higher severity injuries is a common trend.

Furthermore, the liver has been reported to be a common site of abdominal injury, likely a result of its size and anatomical location. Bondy (1980) studied data from the NCSS from January 1977 to November 1979 and found that for AIS 3+ abdominal injuries the most common abdominal injury locations are the liver (30.3%) followed by the kidney (21.9%), spleen (21.6%) and digestive organs (12.3%). Rutledge et al. (1991) analyzed data from patients from the North Carolina Trauma Registry for the years 1987-1990 who were involved in motor vehicle crashes (MVCs). The data set included all trauma patients who were in the hospital for greater than 24 hours or those declared dead in the emergency department. Information was available for 3,901 patients. It was found that the most common abdominal injury locations were the spleen (37%), the liver (29%), the kidneys (17%), and the bladder (8.5%). In the study by Elhagediab, it was reported that the liver was most frequently injured (38%) followed by the spleen (23%) and digestive system (17%). According to a study of abdominal injuries based on the NASS database, the frequency of liver injuries was 15.7% of all abdominal injuries and 34% of AIS 3+ abdominal injuries (Lee and Yang, 2002).

The direction of impact in a MVC is an important factor in determining injury mechanisms, especially when studying abdominal injury where the organs are not symmetrically located. Yoganandan et al. (2000) studied abdominal injuries from MVCs in the NASS/CDS database from 1993-1998. It was found that AIS 3+ liver injuries occur more frequently as a result of right side impacts than left side impacts. This is explained by the location of the liver in

the upper right quadrant of the abdomen and for this reason the study will focus on right side

impacts.

In summary, abdominal injuries are important to study because they often occur in

MVCs and represent a high proportion of serious injuries. The solid abdominal organs are

commonly injured, particularly the liver. Right side lateral impacts are more likely than left side

lateral impacts to cause liver injury and thus the current study will the response of subjects due

to right side loading.

1.2 Anatomy of the Liver

The liver is the largest internal organ in the body with an average weight of 1500 grams.

The liver is essential for metabolism and also is responsible for storage of glycogen and

secretion of bile. The liver is located in the upper right quadrant of the abdomen, inferior to the

diaphragm and deep to ribs 7 through 11, as shown in Figure 1.1. During inspiration, the inferior

edge of the liver moves inferior to the rib cage. The liver and the diaphragm are separated by

peritoneum, a thin serous membrane, except in the bare area of the liver. At the bare area

there is direct contact between the liver and the diaphragm. The liver is located anterior to the

gallbladder and inferior vena cava (IVC).
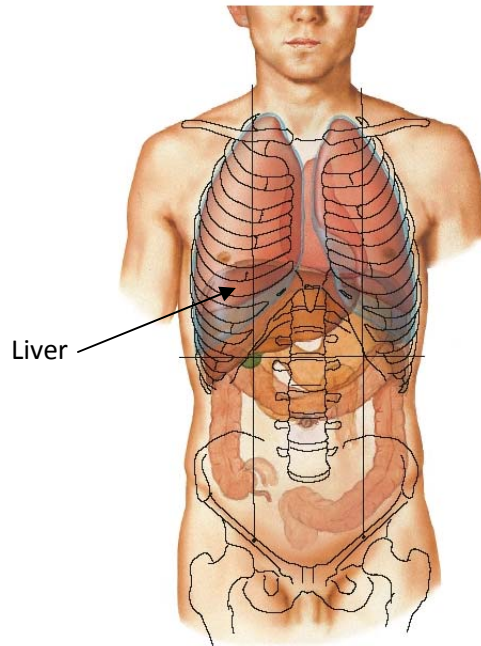
Figure 1.1: Liver Location relative to Abdomen (Netter, 2003)

The liver is supported by five ligaments: the falciform, coronary, left triangular, right triangular and round ligaments. The falciform ligament encloses the round ligament and both ligaments connect the liver to the anterior abdominal wall. On the superior surface of the liver, the triangular and coronary ligaments connect the liver to the diaphragm. The liver is also anchored by the lesser omentum which is a double layer of peritoneum which attaches the lesser curvature of the stomach and the first part of the duodenum. Figure 1.2 and Figure 1.3 show anterior and posterior views of the liver.
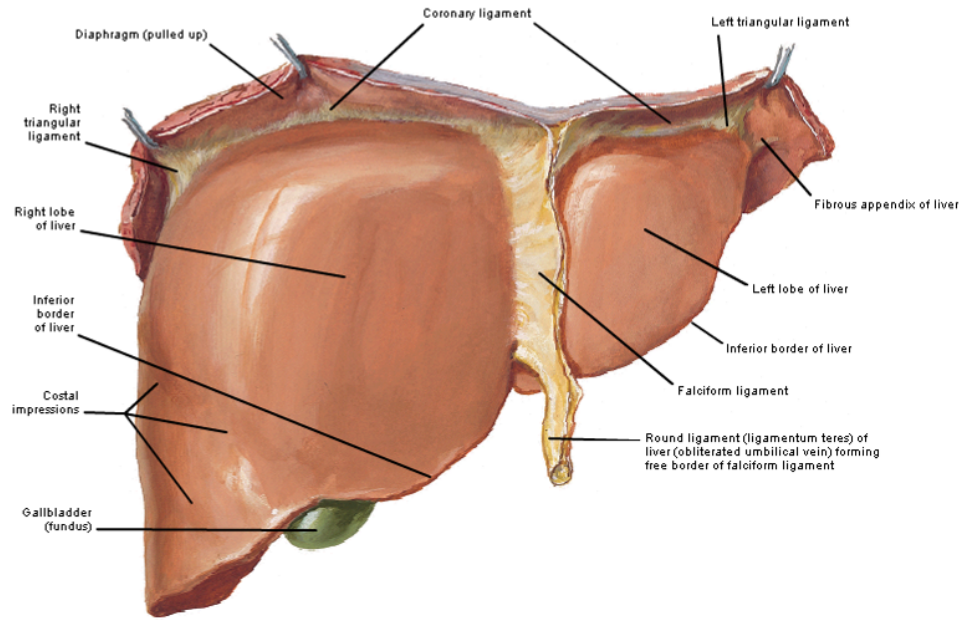
Figure 1.2: Anterior View of Liver (Netter, 2003)
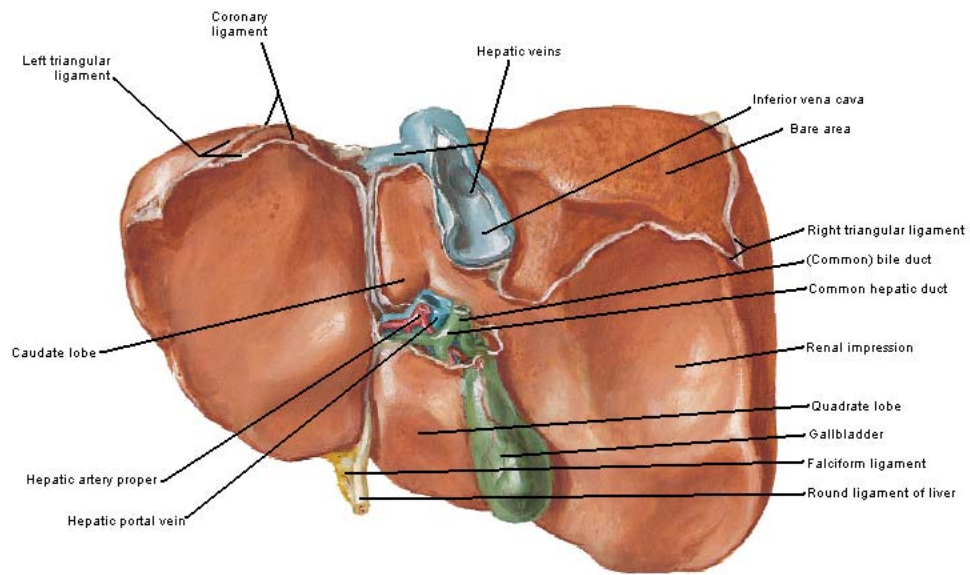
Figure 1.3: Posterior View of Liver (Netter, 2003)

The lobes of the liver are classified by two schemes: anatomical and functional. The anatomical scheme divides the liver into the right lobe, left lobe, caudate lobe and quadrate

lobe. The right lobe is significantly larger than the left lobe and the lobes are divided by the falciform ligament. The caudate lobe is located superior and posterior to the quadrate lobe on the visceral surface of the liver. The caudate and quadrate lobes are divided from each other by the porta hepatis, a transverse fissure and are bordered by the right sagittal fissure and the left sagittal fissure. The right sagittal fissure is composed of the fossae for the gallbladder and the IVC. The left sagittal fissure is the fissure where the round ligament passes through. The portal vein, hepatic artery, bile duct, hepatic nerve plexus, and lymph vessels pass through the porta hepatis. Collectively, the portal vein, hepatic artery, and bile duct are called the portal triad.

The liver can also be divided functionally into two lobes, right and left. The functional lobes are divided by the sagittal plane through the gallbladder fossa and the fossa for the IVC. The functional division of the liver is based on the fact that the right and left functional lobes each have their own blood supply and drainage. The hepatic artery and portal vein each divide into right and left branches to supply the lobes, shortly after passing through the porta hepatis.

The liver receives blood from the portal vein and the hepatic artery, about 70% and 30% of blood by volume, respectively. The portal vein is formed by the junction of the superior mesenteric vein and the splenic vein. The portal vein brings poorly oxygenated blood from the gastrointestinal tract into the liver. The hepatic artery brings well oxygenated blood from the aorta into the liver, via the celiac trunk. The blood exits the liver superiorly through the right, middle or left hepatic vein. The hepatic veins empty into the IVC where the blood is then returned to the heart.

The liver, like many of the abdominal organs, has a high degree of mobility. The serous fluid reduces the friction between the organs and the abdominal walls. Additionally, the liver is not rigidly fixed and the ligaments that tether the liver allow for movement. The position of the

liver depends on the orientation of the subject. For this reason, it is important to consider orientation when performing experimental studies relating to abdominal injury.

1.3 Previous Experimental Work

Many attempts have been made to correlate biomechanical predictors to abdominal injury. Finding a good predictor of injury has clear value in improving current anthropomorphic test devices (ATDs) in order to reduce injuries to the occupant's abdomen in car accidents. Presented here is an overview of correlates that have been studied in the experimental setting for their ability to predict injury. This will provide context for the current study.

Peak applied force has been shown to correlate to abdominal injury in both frontal and lateral testing. The force is typically measured by a load cell behind the impactor face. Trollope et al. (1973) used various sized and shaped impactors to apply a frontal impact to swine (n=15) and monkeys (n=85). It was found that a force of 1.56 kN corresponded to serious injury. In work by Walfisch et al. (1980), post-mortem human surrogates (PMHS) (n=11) were suspended at a height of either one or two meters above a simulated armrest, such that their coronal plane was perpendicular to the ground. The coronal plane is defined as the plane that divides the body into anterior and posterior sections. The subjects were then released and the penetration, load, and contact area was measured. An applied force of 4.5 kN was found to correspond to a 50% risk of AIS 3+ injury. One limitation of this study is that the orientation of the subject could result in the abdominal organs shifting due to their high degree of mobility. Talantikite et al. (1993) performed right lateral impacts with PMHS (n=6). The impacts were centered at 7.5 cm below the xyphoid process, a commonly used positioning for impacts to the upper abdomen. It was found that AIS 3+ injury was well predicted by the applied force (R=0.73). Other studies

also found a correlation between force and injury (Lau, 1981a; Stalnaker, 1973; Rouhana, 1986; Cavanaugh, 1993).

Some studies have looked at peak applied pressure as a predictor of abdominal injury. In experimental work by Melvin et al. (1973), applied pressure was found to be a good predictor of injury in *ex vivo* abdominal organs in monkeys (n=17). For the study, the kidney or the liver in anesthetized subjects was surgically mobilized. The organ was placed on a load cell while continuing to be perfused by the subject. A high speed material testing machine was used to impact the organ at velocities ranging from 12 to 12,000 in/minute. The force-deflection response was measured. It was found that a dynamically applied pressure to the liver greater than 45 psi corresponded to an AIS 3+ injury.

Experimental studies with abdominal organs *in situ* have also shown a correlation between applied pressure and injury. Walfisch et al. measured the load and estimated the contact area to calculate the applied pressure for each subject. A good correlation was shown between applied pressure and AIS 3+ injury (R=0.93). Lau and Viano (1981a) found applied pressure predicted abdominal injury due to belt loading. In their study, anesthetized beagles (n=12) were placed in a supine position. A belt was placed either transversely or diagonally across the subject. The belt loading was applied at 1.7 m/s in the antero-posterior direction producing a nominal 60% compression. The belt force and the belt contact area were measured and the applied force was calculated. It was shown that an applied pressure of 350 kPa produced an injury to the surface of the liver or AIS 2+ liver injury.

Velocity of the applied impact is another predictor that has been studied experimentally. In a study by Stalnaker et al. (1973), PMHS and various monkey species were used to study the side impact tolerance. A pneumatic ram was used to impact the lateral

portion of the upper abdomen at the level of the sixth rib at velocities ranging from 6.1 to 13.1

m/s. Abdominal tolerances for ESI of 3 or higher were found to be 6.1 and 7.3 m/s for the right

and left sides, respectively. Lau and Viano (1981b) subjected New Zealand white rabbits (n=26)

to blunt abdominal impacts, applied by a pneumatic impactor. The antero-posterior

compression was held constant (16%) while velocities ranged from 5 to 20 m/s. It was found

that liver injury consistently increased with increasing velocity. Additional studies have also

concluded velocity is a good predictor (McElhaney, 1971; Prasad, 1984). Impact velocity is

related to the energy input into the system which may explain its strength as a biomechanical

predictor of injury.

Additionally, experimental work has used maximum normalized deflection, referred to

as compression, to predict injury. In Horsch et al. (1985), anesthetized swine (n=17) were

suspended from a test frame in a seated position. A steering wheel column was aligned such

that the lower rim would contact the area of the abdomen over the liver. A pulse was applied to

the test frame and injuries were documented. The measured peak abdominal compression

related to the abdominal injuries sustained by the subject (R=0.62). Viano et al. (1989) impacted

unembalmed cadavers (n=14) at 30 degrees from lateral through the center of gravity of the

liver. High speed video was used to capture the deflection of the abdomen. It was found that a

compression of 44% correlated to injury. Miller (1989) used swine (n=25) to study the

biomechanical response of the lower abdomen. The subjects were anesthetized and subjected

to simulated belt loading with loading velocities ranging from 2 to 7 m/s. A 50 percent risk of

AIS 3+ abdominal injury was predicted by a compression of 48%. Kent et al. (2008) used the

abdomen of post-mortem swine (n=47) as a model for the pediatric abdomen. Belt loading was

applied using a pneumatic piston/cylinder assembly. Some subjects were subjected to ramp and

9

release loading while others were subjected to ramp and hold loading. Maximum compression

was shown to predict injury well for loading rates up to and higher than 7.3 m/s.

Most studies used normalized deflection, compression, as a predictor of abdominal

injury but Talantikite et al. (1993) found that non-normalized deflection was a better injury

predictor than compression. In the study, PMHS (n=6) were subjected to right lateral impacts

with the impact at the level of the liver. An external mechanical system consisting of two

potentiometers was used to measure the deflection. The study showed that injury and

deflection were well correlated (R=0.81) but that compression did not strongly relate to injury.

Another biomechanical predictor that has been proposed is the Abdominal Injury

Criteria (AIC). The AIC is calculated by multiplying the maximum velocity of the impactor by the

maximum compression obtained. It is commonly written $V_{max}*C_{max}$. It should be noted that the

maximum velocity and the maximum compression do not have to, and likely will not, occur at

the same point in time. Since compression is unit-less, the units of the AIC are the same as

velocity, usually reported as meters per second. The AIC has been shown to relate to thoracic

injury severity (Viano, 1983) and abdominal injuries (Rouhana, 1985). In the Rouhana study,

New Zealand white rabbits (n=117) were placed in a sling in the prone position and a pneumatic

impactor was used to laterally impact the subject over the 12th rib. The tests were conducted at

velocities from 3 to 15 m/s and resulted in compressions of 10% to 50%. It was shown that AIC

related well to injury (R=0.85 for left-side impacts and R=0.84 for right-side impacts).

Supporting evidence for $V_{max}*C_{max}$ as an injury criteria has been reported by various studies

(Stalnaker, 1985; Rouhana, 1986; Rouhana, 1987).

The viscous criterion (VC) was proposed by Viano and Lau (1986) and has also been

shown to predict abdominal injury well. The VC is given by the maximum of the product of the

velocity time history and the compression time history. The viscous criterion is commonly

written as $[V(t)*C(t)]_{max}$ or VC_{max}. The units of the viscous criteria are the same as velocity,

similar to the abdominal injury criteria. In the PMHS study, Viano et al. (1989) found that for an

abdominal side impact to a PMHS, a VC of 1.98 m/s corresponds to a 25% risk of AIS > 4 injury.

Miller (1988) reported that for belt loading of swine, a VC of 1.40 m/s corresponded to a 25%

risk of AIS > 4 injury. Talantikite (1993) found that for lateral impacts to PMHS, VC showed a

strong (R=0.71) relationship to injury severity. Other researchers have found similar results

correlating injury to the viscous criterion (Cavanaugh, 1993; Kent, 2008).

Another factor that has been identified as predicting abdominal injury is the maximum

force times the maximum compression, such as in the study by Miller (1989). Similar to the AIC,

the peak force and maximum compression do not necessarily occur at the same time. A strong

correlation was shown for AIS 3+ (0.67) and AIS 4+ (0.71) injuries. Building off of this previous

work, Kent et al. (2008) showed a good correlation between injury and both the belt force and

the reaction force. In this study, it was also proposed to use the maximum of the rate of change

of force multiplied by the compression time history ($[\dot{F}(t)*C(t)]_{max}$). He termed this the kinetic

analog to the viscous criterion (KVC). The justification for use of this term is that, "the rate at

which the applied force changes with time ... reflects a characteristic of the structure being

loaded, not just the test input condition."

Studies have also been done to study the relationship between internal pressure and

injury. Williams and Sargent (1963) applied a force of 1780 N to the abdomens of anesthetized

dogs using a drop tower. The pressure in the peritoneum and the gastrointestinal tract was

measured. The peak pressure in the peritoneum was higher than in the intestine. These results

did not support the hypothesis that intestinal injury was the result of higher pressure in the

intestines than in the peritoneum. The study did not show a link between pressure and

abdominal injury. Rouhana et al. (1986) also concluded that the pressure did not correspond to

injury based on impacts of white New Zealand rabbits. The specimens were impacted at

velocities between 5 and 15 m/s. A total of 120 specimens were tested using a pneumatic ram

with a rigid face. The pressure measured in the esophagus and the femoral artery was found to

have no correlation to injury. However, no pressure transducers were placed in the solid organs

or in the venous vasculature.

However, Lau and Viano (1981b) also investigated abdominal injury using white New

Zealand rabbits. A pressure sensor was placed in the esophagus at mid thoracic level and the

impact was applied at velocities from 5 to 20 m/s. In this study, esophageal pressure showed a

strong (R=0.76) correlation to abdominal injury. Prasad and Daniel (1984) also found a

relationship between injury and blood pressure measured in the descending aorta when

performing high speed accelerations on anesthetized piglets. It was found that blood pressure

peaks greater than 53.3 kPa are associated with AIS 3+ injuries. Miller (1989) placed sensors in

the right carotid artery and the jugular vein of swine to measure the arterial and venous

pressure. Occurrence of AIS 3+ injuries generally increased with higher measured pressures.

These studies all use human surrogates to study abdominal injury. The advantage of

experimental work using human surrogates is that it is not necessary to artificially perfuse the

abdomen. However, it is not clear if the relationships to abdominal injuries observed in the

human surrogates are also true in humans.

Sparks et al. (2007) used *ex vivo* human livers to study internal pressure as an injury

predictor. Rigid plate, drop tower impacts were performed to fourteen human liver specimens.

During the testing, the venous and arterial systems were perfused with saline to physiological

pressures. The internal vascular pressure of the fluid was measured as well as the tissue

pressure in the liver parenchyma. The location of the vascular pressure sensor varied from liver

to liver. To compare the tests, a midline vascular pressure was calculated using the radial

distance from the impact, to account for the geometric location, and the strain rate, to account

for the variation in velocities. A midline vascular pressure of 64 kPa correlated with a 50%

chance of AIS 3+ injury and was found to predict injury well (p<0.02).

1.4 Goals of Current Work

Pressure has been measured in some full body PMHS experimental work (Cavanaugh,

1986; Nusholtz, 1980) but the results were insufficient to link pressure changes to injury. The

current research seeks to provide a better understanding of the link between pressure and

injury by testing the human liver *in situ* with boundary conditions more representative of real

world trauma.

Pressure provides many advantages over other abdominal predictors. First, pressure

measurements are independent of the direction of impact which may be an advantage of using

pressure when creating an ATD abdomen that could be used in crash testing. The direction of

applied force may not be known but a pressure measurement may help characterize external

forces or energy. The pressure is also related to stress which can be difficult to measure in soft

tissues. Additionally, pressure measurements from PMHS may help improve finite element

models of the abdomen since the sensors can provide localized measurements of the loading. If

a correlation is found between pressures or pressure related variables and injury, the variables

could be measured in FE models to predict injury.

Pressure has clear advantages as an abdominal injury predictor so the main focus of the study is the relationship between injury and pressure with the following goals:

- Measure pressure changes in the vasculature of full-body post mortem human subjects in response to impact

- Determine if the measured pressure changes can be used to predict injuries to the abdomen in full body PMHS

- Relate the findings from the *in situ* liver testing to previous work done with *ex vivo* livers in an effort to better understand the role of the boundary conditions in impact

In addition, secondary goals of the work will include the following:

- Investigate previously used biomechanical predictors for abdominal injury and compare results from the current study

- Evaluate the thoraco-abdominal response of the PMHS in full body, rigid impacts

Chapter 2: Methods

2.1 PMHS Selection and Preparation

For the testing, PMHS (n=6) were obtained through the willed body donation program

at Ohio State. Both males and females were accepted for testing and all subjects met the

following criteria:

- **The subject had a body mass index (BMI) between 18.5 and 30 kg/m^2**. This means the PMHS was classified as normal or overweight, according to the World Health Organization ("Obesity…", 2000) BMI is given by the following calculation:

$$BMI = \frac{\text{weight in kg}}{(\text{height in meters})^2}$$

- **The subject was not osteoporotic, according to the whole body Dual Energy X-ray Absorptiometry (DXA) bone scan**. This corresponds to a T-score of greater than -2.5. A T-score is the number of standard deviations a person is below the average bone density of a healthy adult of 30 years old of the same gender.

- **The subject did not have scars indicating major abdominal surgery.** It was acceptable if the subject's gallbladder had been removed.

- **The subject did not weigh more than 95 kg.** A subject that weighed more than 95 kg would have been difficult to transport and position.

If the PMHS was acceptable, the tests were performed within four days of death. The subjects

were not frozen prior to testing but were kept at 4 degrees Celsius to prevent tissue degradation.

A summary of the tests and subject data is given in Table 2.1. More anthropometry

measurements are provided in Appendix A.

15

Table 2.1: Summary of Test Data

	FBL01-L	FBL02-L	FBL03-L	FBL04-L	FBL05-O	FBL06-O	Average	Standard Deviation
Impact Direction	Lateral	Lateral	Lateral	Lateral	Oblique	Oblique	--	--
Gender	Male	Female	Male	Male	Female	Male	--	--
Age	68	80	88	91	53	79	76.5	$\pm$ 14.0
Mass (kg)	67	59	73	64	54	82	67	$\pm$ 10
Stature (cm)	176	154	188	179	164	179	173.3	$\pm$ 12.2
Chest Breadth (cm)	26.9	30.8	27	27.3	30	30.8	28.8	$\pm$ 1.9
Waist Breadth (cm)	25.8	33	30	29.5	30	35	30.6	$\pm$ 3.2
Seated Height (cm)	93.5	87	96	97	91.5	99	94	$\pm$ 4.3
Impact Velocity (m/s)	7.2	7.09	7.03	7.06	7.13	7.03	7.09	$\pm$ 0.07
BMD (g/cm^2)	1.293	1.008	1.139	1.095	1.039	1.308	1.100	$\pm$ 0.13
T-score*	0.9	-1.5	-1	-1.6	-1.1	1.1	-0.5	$\pm$ 1.2

T-Score measured by Dual energy X-ray absorptiometry (DXA). -1.0 or higher: Normal bone mass density, -2.5 to -1.0: Osteopenic, -2.5 or lower: Osteoporotic

2.2   Internal Instrumentation

The goal of the instrumentation was to measure the change in pressure during impact while pressurizing the abdomen to physiological pressures. To accomplish this, the abdominal aorta and the inferior vena cava were blocked superior and inferior to the abdomen. Pressure sensors were inserted into the vessels and saline was used to pressurize the vessels before impacting the right side of the PMHS. A fluoroscope was used to provide real time imaging of the locations of the sensors and the occluding balloons.

In order to measure the pressure in the vessels, micro-pressure transducers (Millar Instruments model SPR-524, Houston, TX) were used. The transducer is 1.17 mm in diameter (3.5 French (Fr)) and the wire leading to the transducer is 0.77 mm (2.3 Fr). The sensors can operate in fluids and have a frequency response of 10 kHz. One or two pressure transducers were attached to the outside of a 5 Fr angiographic catheter using shrink wrap. The purpose of the angiographic catheter was to provide stability to the sensors when inserted in the vessels. For each test, a total of four angiographic catheters were prepared. In most cases, if two sensors were used they were located approximately 1 cm apart to provide a redundant measurement of the pressure at that location. Each angiographic catheter with the attached pressure sensor(s) was inserted into a Foley catheter. The tip of the Foley catheter was removed and the pressure transducers were extended beyond the end of the Foley catheter, as shown in Figure 2.1. The Foleys had a 30 cc balloon, shown in Figure 2.2, which was used to occlude the vessels. The size of the Foley catheters used depended on the size of the subject's vessels and ranged from 16 to 20 Fr.
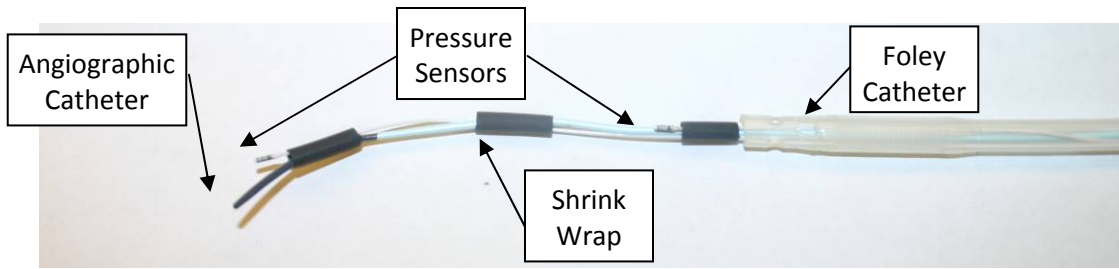
Figure 2.1: Foley Catheter with Instrumentation Inserted

Figure 2.2: Inflated Foley Balloon

In order to block the abdominal aorta and inferior vena cava inferiorly, an incision was inferior to the inguinal ligament and the femoral artery and vein were dissected. Along each vessel, an incision was made length-wise, being careful not to completely transect the vessel. The vessels were tied off inferior to the incision to prevent blood from the lower limb from leaking at the site of the incision. For the arterial instrumentation, a Foley catheter with inserted instrumentation was inserted into the femoral artery and the Foley balloon was used to occlude the descending aorta superior to the bifurcation of the iliac artery. Similarly on the venous side, the instrumentation was inserted into the femoral vein and the Foley balloon was used to occlude the inferior vena cava proximal to the bifurcation of the iliac veins. Strings were tied around the vessels and Foley catheters to hold the catheters in place. The incision was sutured closed and the Foley catheters were sutured superficially to the skin to prevent the catheters from moving internally while positioning the body.

In order to occlude the descending aorta superiorly, various paths were taken to locate the Foley and the instrumentation. In test FBL01-L, the left brachial artery was dissected out and the instrumentation was inserted through the left subclavian artery and the aortic arch and into the superior descending aorta. In test FBL02-L, the left carotid artery was used because the brachial artery was too narrow for the Foley catheter to pass through. In test FBL03-L, FBL04-L, FBL05-O and FBL06-O, an incision was made directly into the left side of the arch of the aorta in order to place the sensors in the descending aorta. In all cases, the instrumentation was inserted and the Foley balloon was inflated to occlude the vessel superior to the diaphragm.

For occlusion of the inferior vena cava superiorly, the right internal jugular vein was dissected out by making an incision anterior to the sternocleidomastoid muscle. The Foley catheter was directed through the right atrium of the heart and the Foley balloon was in the IVC between the heart and the hepatic veins. The instrumentation was extended beyond the tip of the Foley catheter and directed rightward into a hepatic vein. The sensors were inserted as far as possible into the vein. Quantification of the sensor locations will be presented later.

For the superior instrumentation catheters, a "Y" pipe fitting was connected to the Foley. One input port was used to insert the instrumentation through the Foley catheter. A compression fitting was used to prevent saline from exiting through that port during testing. The other input port was temporarily capped and was connected to the saline reservoir directly prior to testing. Figure 2.3 is a picture of the output port.
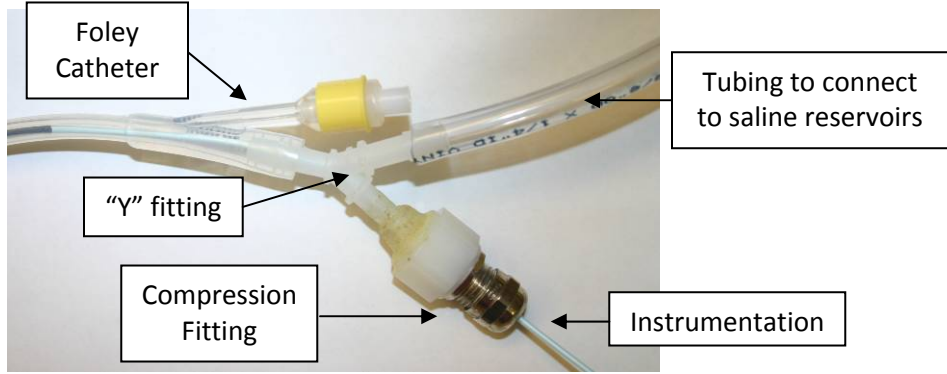
Figure 2.3: Example of Foley Catheter Output Port

A schematic of the desired instrumentation locations and blockages is given in Figure

2.4. However, it was not always possible to achieve these locations due to variable anatomy,

blockages, or incorrect identification of structures. A summary of these issues will be presented

in the results section.
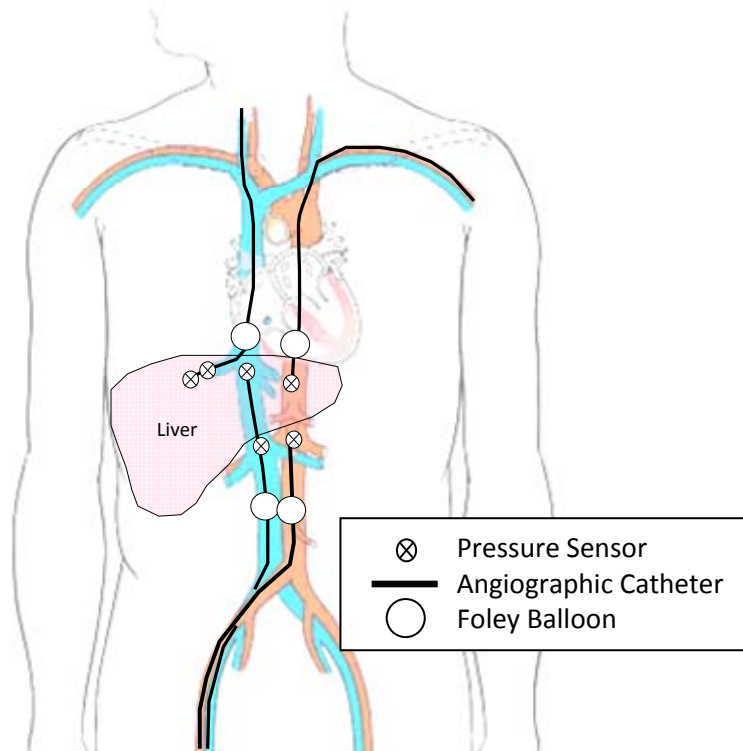
Figure 2.4: Desired Internal Instrumentation of PMHS

Following internal instrumentation, a Computed Tomography (CT) scan was taken of the subject's thorax and abdomen. The CT scan was used to document the locations of the internal instrumentation and the pre-impact anatomy, particularly pre-existing conditions and anomalies of the liver.

2.3 External Instrumentation

Using a fluoroscope, the vertebral levels of T1, T8, and T12 were identified so instrumentation could be placed at these levels. The levels were selected because they correspond to accelerometer locations that commonly are measured in ATD testing. The PMHS was placed in the prone position and at each of the identified sites part of the spinous process of the vertebral bodies was removed. A mount was rigidly attached to the vertebral body using a long screw through the neural arch and into the vertebral body. A block with three accelerometers and three angular rate sensors, as shown in Figure 2.5, was then attached to each mount on the spine. This block is also referred to as a 3aω block. The six sensors allow for the six degrees of freedom of the block to be measured. A mount was also attached to the sternum using two screws through the body of the sternum and a 3aω block was also attached to this mount.
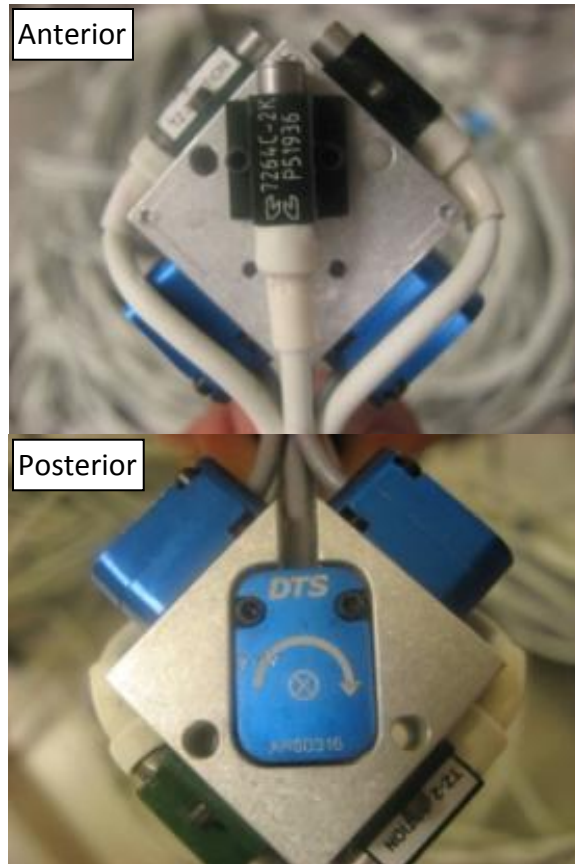
Figure 2.5: 3aω Block

A 40-channel chestband was placed around the subject and secured externally using tape such that the chestband was centered at the level of impact. The chestband is a measurement device that consists of strain gauges bonded to a thin metal band protected by a layer of rubber. The strain gages measure the strain which can be used to calculate the deflection of the chest during impact. The use of the chestband to measure deflections during lateral impacts has been shown to be valid (Pintar, 1997). When aligned with the center of the impactor, the chestband typically was located between the instrumentation on T8 and T12. A schematic showing the external instrumentation is shown in Figure 2.6.
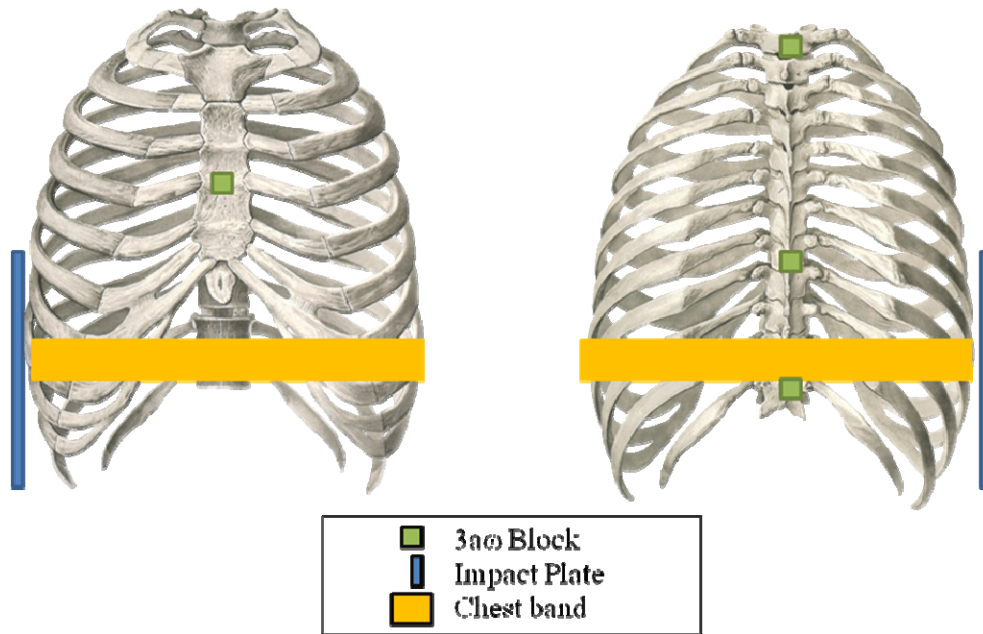
Figure 2.6: External Instrumentation

2.4 Test Preparation

The subject was positioned on a lift table in front of a pneumatic ram and the inferior edge of the rib cage at the right mid-axillary line, typically rib eleven, was aligned with the bottom edge of the aluminum impactor plate. This alignment was selected because the liver is located directly behind the ribs and at the inferior edge of the rib cage.   A total of four lateral tests and two oblique tests were performed. For the lateral tests, the mid-axillary line was aligned with the center of the plate. For the oblique tests, the subject was rotated 30 degrees towards the impactor such that the impact line was through the vertebral body, as in Figure 2.7.
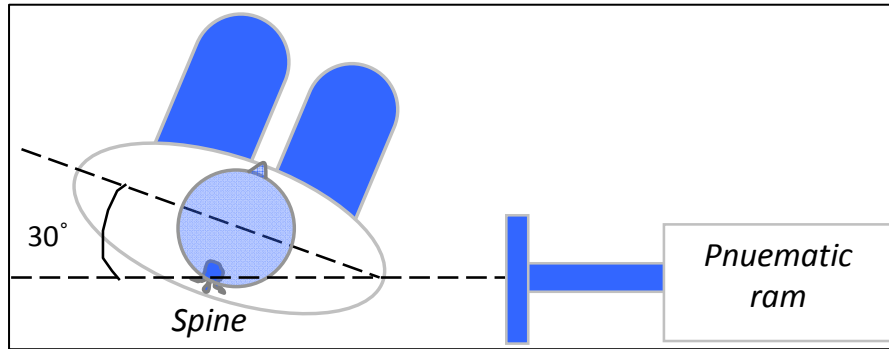
Figure 2.7: Overhead View of Oblique Impact

Prior to impact, the subject's lungs were inflated to about 6 kPa through an intubation tube inserted through the trachea. The arms were crossed and secured on a platform at shoulder level, parallel to the ground, to avoid the arms interfering with the impact. Figure 2.8 and Figure 2.9 show example pretest positioning of the subjects in the lateral and oblique tests respectively.
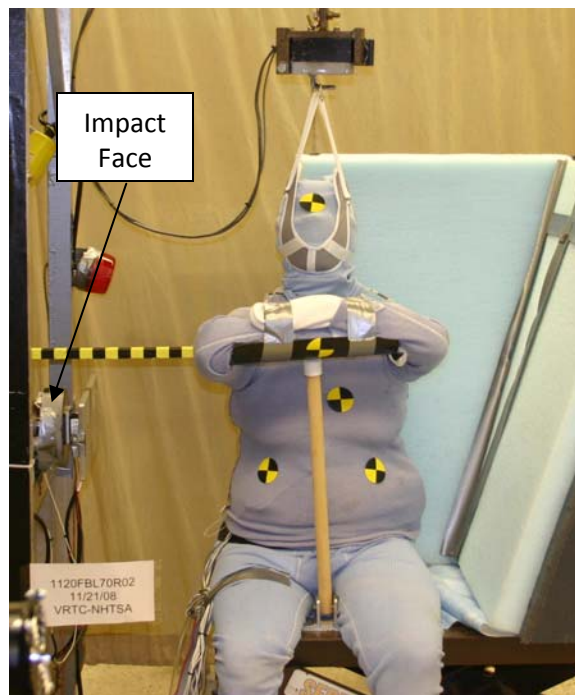
Figure 2.8: Pre-test Positioning of Lateral Impact

Figure 2.9: Pre-test Positioning of Oblique Impact

Event tape was placed on the subject and ram which provided a time marker for when

the ram and the subject were in contact. The impactor plate was made out of aluminum and

was 15 cm high and 30 cm wide with a mass of 1.59 kg. The total ram mass was 23.97 kg. When

the subject was in final position, anatomical landmarks and the locations of the 3aw blocks were

digitized using a point digitizing arm (Faro Technologies Inc., Lake Mary, FL). This allowed for

the acceleration and the rotation of the vertebral bodies to be calculated relative to the body

coordinate system which was different than the coordinate system in which the measurements

were taken. A secondary impact protection unit which has two sides and is covered in foam was

secured to the table to catch the PMHS following impact. This eliminated the possibility of

further injuries not caused by the impact event.

Prior to testing, the subjects' abdominal vasculature was pressurized using saline. The

saline was placed in reservoirs at two different heights in order to obtain physiological pressures

in the vasculature. The arterial reservoir was located 130 cm above the center of the impact

face, corresponding to a pressure of 96 mmHg at the level of the center of the impact plate.

This is in the range of normal systolic blood pressure which is between 80 and 120 mmHg

(Guyton, 1976). The venous reservoir was located between 9 and 33 cm above the center of the

ram. These heights correspond to pressures between 6.7 and 24.4 mmHg.   The typical value of

pressure in the right atrium is 5 mmHg (Guyton, 1976).   A slightly higher pressure was used for

pressurization of the hepatic veins in order to increase the likelihood of pressurization of the

veins.

It should be noted that the portal system was not pressurized. The subjects would have

had some blood remaining in the portal system but accessing the portal system for further

pressurization would have required extensive disruption of the abdomen. It was decided that

minimizing incisions into the abdomen was more important than pressurizing the portal system,

especially since the typical pressure levels in the portal system are relatively low at only 8-10

mmHg.

In test FBL05-O and FBL06-O, one or two pressure sensors were inserted directly into

the liver parenchyma. To access the liver tissue, an incision was made through the skin,

subcutaneous tissue, intercostal muscles, and the diaphragm between ribs 7 and 8 or ribs 8 and

9 on the posterior lateral aspect of the thorax. For placement of the sensors, a needle was

inserted into the liver tissue and then removed. The sensor was inserted into this hole and the

depth of the sensor was recorded. The sensor was super glued into place at the location where

the sensor wire exited the liver. The incision was sutured closed and the sensor wire was

superficially tethered to the subject.

The reservoirs each contained a pump which kept the water height at a consistent level. Tubing was used to connect the reservoirs to the PMHS and the air was bled from the tubing prior to testing. The length of pressurization ranged from 3 to 5 minutes. On the venous side, the height on the reservoir was increased initially to move the saline through the tubing but was returned to the predetermined height during impact. A schematic of the setup is shown in Figure 2.10.
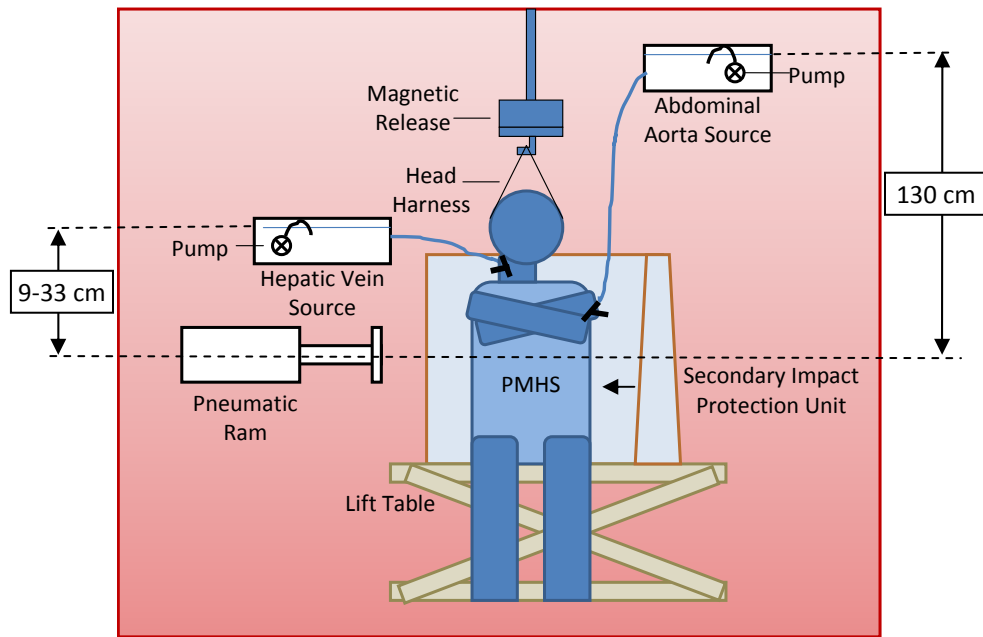
Figure 2.10: Schematic of Setup

For the test, data signals were collected using a data acquisition system (Yokagawa Electric Corporation, Tokyo, Japan). A high speed video camera was used to record the frontal view, perpendicular to the impact at a rate of 1000 frames per second. The nominal impact velocity was 7.0 m/s. Just prior to impacting the subject, a magnetic bracket released the subject's head restraint such that the subject was upright at the time of impact without the head motion being restricted. Following the impact, a computed tomography scan on the subject was taken. An autopsy on each subject was performed to document injuries.

2.5 Data Processing

The frequency of the data acquisition was 20,000 Hz. A pre-filter of 3000 Hz was applied

to eliminate high frequency noise. Then, the data signals were filtered according to standard

SAE-J211. Next, any offset in the data channels before initiation of the channel was set to zero

by subtracting the bias.

2.6 Quantification of the Pressure Sensor Locations

The pre-test computed tomography (CT) scans of the subject were used to identify the

locations of the pressure sensors in the subject relative to the impactor plate. The location

where the bottom edge of the impact plate contacted the subject was found by identifying the

lowest cross sectional slice at which the right side rib eleven was still visible. This corresponds

to the lowest point of the rib cage at the mid-axillary line. Since the CT slices were taken at 1

mm slices, the slice corresponding to the center of the impactor plate was identified as the slice

that was 151 slices (151 mm) above the slice at the bottom edge of the impactor plate. The

location of the instrumentation was found for each sensor. A linear distance was measured

from the point where the impactor would first contact the subject to the instrumentation in the

direction of the impact. The superior-inferior distance between the center of the ram and the

instrumentation site was also measured. Using these distances, a resultant distance between

the center of the ram and the instrumentation site was found. For the lateral tests, this line was

in the coronal plane of the body. For the oblique tests, the distance was in the plane 30 degrees

from the coronal plane, perpendicular to the impactor face.

2.7 Transformations

After initial processing, the acceleration and angular rate sensor signals from the blocks

on the spine and the sternum were transformed to the laboratory coordinate system. The

transformed acceleration was double integrated to obtain the translation of the subject. The

angular velocity was integrated to obtain the angular displacement. The explanation of the

transformation and the computer code used for computation is given in Appendix B. The

transformed accelerations were used in the normalization of the data.

2.8 Normalization

Since the subject anthropometry was different for each test, the forces, times, and

displacements were normalized to allow for more meaningful comparison of the data. There

are two methods which are commonly used to scale biomechanical data.

The first type of normalization is mass-based scaling, as proposed by Eppinger et al.

(1984).   It assumes that the subjects have a constant density and stiffness. The subjects are

scaled based on a ratio of the subject's whole body mass divided by the body mass of the 50th

percentile subject. One major limitation of this method is that it does not take into account that

subjects have different proportions, even if they have the same mass. Two subjects might have

the same mass and therefore scaling factors but one may be tall and slender while the other

may be shorter and obese.

Another normalization scheme, Impulse-Momentum Based Scaling, was proposed by

Mertz (1984). This technique uses a stiffness ratio and a mass ratio but the mass ratio is based

on a calculated effective mass from the data collected during the test. The two-body impulse-

momentum normalization technique, such as for pendulum or ram tests, was proposed by Viano

et al. (1989). For this, the effective mass for each test was calculated as follows:

(2.1)
$$m_{eff} = \frac{m_p(\int_0^T a_p dt)}{(\int_0^T a_{sub} dt)}$$

29

where

m_p = mass of the pendulum
a_p = acceleration of the pendulum
a_{sub} = acceleration of the subject
T = time of maximum deflection
0 = time zero, defined as time of initial contact between the ram and the subject

The variable T was measured by the chestband in all tests except FBL02-L. In FBL02-L,

some of the chestband signals were clipped so the maximum time of deflection was instead

measured by double integrating the accelerometers on the ram and on vertebral level T8 to get

the displacements. These were subtracted and the time of the maximum compression was

identified.

Using the effective mass, a mass ratio for the lateral tests and a mass ratio for the

oblique tests were calculated by:

(2.2)
$$R_m = \frac{(m_{eff})_{50th}}{(m_{eff})_{sub}}$$

where

$(m_{eff})_{50th}$ = the standard effective mass
$(m_{eff})_{sub}$ = the effective mass of the subject

The standard effective mass was found by calculating the ratio of effective mass to total

body mass for each subject and averaging the results for the lateral and oblique tests. This

value was multiplied by 76 kg, representing the standard whole body mass of a 50th percentile

male.

Assuming that the subject stiffness is proportional to the chest breadth, the stiffness

ratio was calculated by:

$$R_k = \frac{K_{50th}}{K_{sub}}$$

(2.3)

where

K_{50th}= the chest breadth of an average subject (34.9 cm)
K_{sub}= the chest breadth of the subject

Chest breadth was selected to define the stiffness because the impact was to the lower

rib cage and the chest breadth was the most consistent anthropometric measurement near the

impact site.

The scaling factors are given by the following relationships:

Displacement

(2.4)

$$R_D = \frac{V_{50th}}{V_{sub}} \frac{\sqrt{R_m}}{\sqrt{R_k}} \sqrt{\frac{m_p + m_{50th}}{m_p + m_{sub}}}$$

Time

(2.5)

$$R_T = \frac{\sqrt{R_m}}{\sqrt{R_k}} \sqrt{\frac{m_p + m_{50th}}{m_p + m_{sub}}}$$

Force Factor

(2.6)

$$R_F = \frac{V_{50th}}{V_{sub}} \sqrt{R_m R_k} \sqrt{\frac{m_p + m_{50th}}{m_p + m_{sub}}}$$

where

V_{50th}= velocity of 50th percentile subject
V_{sub}= velocity of subject
R_m= mass ratio
R_k= stiffness ratios
m_p= mass of the pendulum
m_{50th}= mass of 50th percentile subject
m_{sub}= mass of subject

31

2.9 Calculating Biomechanical Variables

As discussed earlier, various biomechanical variables have been proposed in the past as predictors of abdominal injury. Table 2.2 provides a summary of how the variables were calculated from the collected data.

Table 2.2: Calculation of Biomechanical Variables

Variable	Units	Method of calculation
Displacement (d)	mm	• Process chestband data using numerical computation software (Matlab, Natwick, MA) • Identify the gages initially at the mid-axillary lines • Calculate compression between gages as a function of time • Report maximum displacement from original position at time zero
Compression (c)	unitless	• Normalize the displacement by the chest breadth of the subject as calculated by the initial position of the mid-axillary chestband gages
Abdominal Injury Criterion ($V_{max}*C_{max}$)	m/s	• Multiply the velocity of the ram at the time of the event (t=0) by the compression • Report the maximum
Viscous Criterion ($[V*C]_{max}$)	m/s	• Obtain the time history of compression from the chestband • Differentiate the compression using a 5-point central difference equation to obtain velocity of compression $$f'(x)= \frac{-f(x+2h)+8*f(x+h)-8*f(x-h)+f(x-2h)}{12h}$$ • Multiply compression by velocity • Filter at calculated signal at 1000 Hz • Report the peak value
Kinetic Viscous Criterion (KVC) ($[\dot{F}C]_{max}$)	N/ms	• Filter the ram acceleration at 100 Hz • Zero at time=-0.09, prior to ram movement • Multiply acceleration by the mass of the ram • Differentiate the force using the 5-point central difference formula • Multiply the rate of change of force by the compression • Report the peak value
Peak Change in Pressure (P_{max})	kPa	• Filter raw pressure signal at 1650 Hz • Zero at time=-0.01 seconds • Report maximum change in pressure
Peak Rate of Change of Pressure ($\dot{P}_{max}$):	kPa/ms	• Filter raw pressure signal at 1650 Hz • Zero at time=-0.01 seconds, differentiate using 5-point central difference formula • Report maximum rate of change of the pressure
Peak Rate of Change in Pressure times Peak Pressure ($P_{max}\dot{P}_{max}$):	kPa^2/ms	• Filter raw pressure signal at 1650 Hz • Zero at time=-0.01 seconds, find maximum of pressure, differentiate pressure using 5-point central difference formula • Find maximum rate of change • Multiply the maximums • Report value for each set of pressure data
Peak of Rate of Change in Pressure times Pressure ($[\dot{P}P]_{max}$):	kPa^2/ms	• Differentiate using 5-point central difference formula • Multiply pressure times the rate of change of the pressure • Report maximum

2.10 Statistical Analysis of Binary Regression

The pressure related variables were analyzed for their predictive capability using a

binary logistic regression model. Variables were considered significant if $p \leq 0.05$. The log

likelihood was used to evaluate which predictor variables best fit the data. Log likelihood ranges

from negative infinity to 0 and is a useful tool to compare predictors with gamma values closer

to zero indicating a stronger predictor. Additionally, the Goodman and Kruskal's Gamma (γ) was

used to access the model's predictive ability, similar to work by Kent et al. (2008). To calculate

gamma, the predictor variables were classified into groups of injurious or non injurious based on

AIS. The predictor variable was then used in the model to determine if the model predicted

injury or non-injury was more likely for that input value. If the experimental result agreed with

the most likely outcome from the model, the data point was concordant. If the experimental

result disagreed with the most likely outcome from the model, the data point was discordant.

Gamma was found by:

(2.7)
$$\gamma = \frac{N_C - N_D}{N_C + N_D}$$

where

N_c= the number of concordant points
N_d= the number of discordant points

The values of gamma range from 0 to 1 with values closer to 1 meaning the model has

better predictive capability.

Chapter 3: Results

3.1 Injury Analysis

The autopsy performed following each test focused on identifying muscular

damage, injury to skeletal structures, and abdominal injury, particularly to the liver. The

injuries were graded using the Abbreviated Injury Scale (AIS). Table 3.1 provides a

summary of the AIS ratings for injuries to the liver. Table 3.2 summarizes the autopsy

results from each test with complete results given in Appendix C.

Table 3.1: Summary of AIS Ratings for Liver Injuries

AIS Rating	Description
0	No injury
2	Superficial Lacerations Hematoma < 50% surface area or intra-parenchymal $\leq$ 10 cm in diameter
3	Laceration with duct involvement and > 3cm parenchymal depth Hematoma > 50% of surface area
4	Multiple deep lacerations Parenchymal disruption of $\leq$ 75% of a hepatic lobe Burst injury
5	Parenchymal disruption of >75% of a hepatic lobe or involving vascular attachments of the liver Pulpefication
6	Hepatic Avulsion

Table 3.2: Summary of Autopsy Results

Test Number	Ribs		Liver		Lungs	
	Injury Description	AIS Level	Injury Description	AIS Level	Injury Description	AIS Level
FBL01-L	Fractures of ribs 5 and 6 on the right side	2	Minor laceration on the right inferior aspect of the liver	2	none	0
FBL02-L	Fractures on ribs 2-12 on the right side and ribs 2-4 and 7 and 8 on the left side, bi-lateral flail chest	5	none	0	Lung contusion on the right side with pneumothorax	3
FBL03-L	Fractures on ribs 6-11 on the right side, unilateral flail chest	3	Burst injury to the liver on the posterior side of the liver, primarily to the right lobe of the liver	4	none	0
FBL04-L	Fractures of ribs 3-12 on the right side and ribs 9 and 10 on the left side, unilateral flail chest	3	none	0	none	0
FBL05-O	Fractures of right ribs 4 through 8, unilateral flail chest	3	Lacerations on anterior and posterior right lobe, areas of capsular damage	2	none	0
FBL06-O	Fractures of right ribs 3 through 10, unilateral flail chest	3	Three transverse lacerations across anterior surface of liver, right lobe tissue disruption	2	none	0

Three tests (FBL01-L, FBL05-O, and FBL06-O) resulted in lacerations to the liver. Test

FBL03-L resulted in a serious liver injury to the right lobe. This was the only serious injury that

was obtained from the testing. Figure 3.1 shows images depicting the locations of the rib
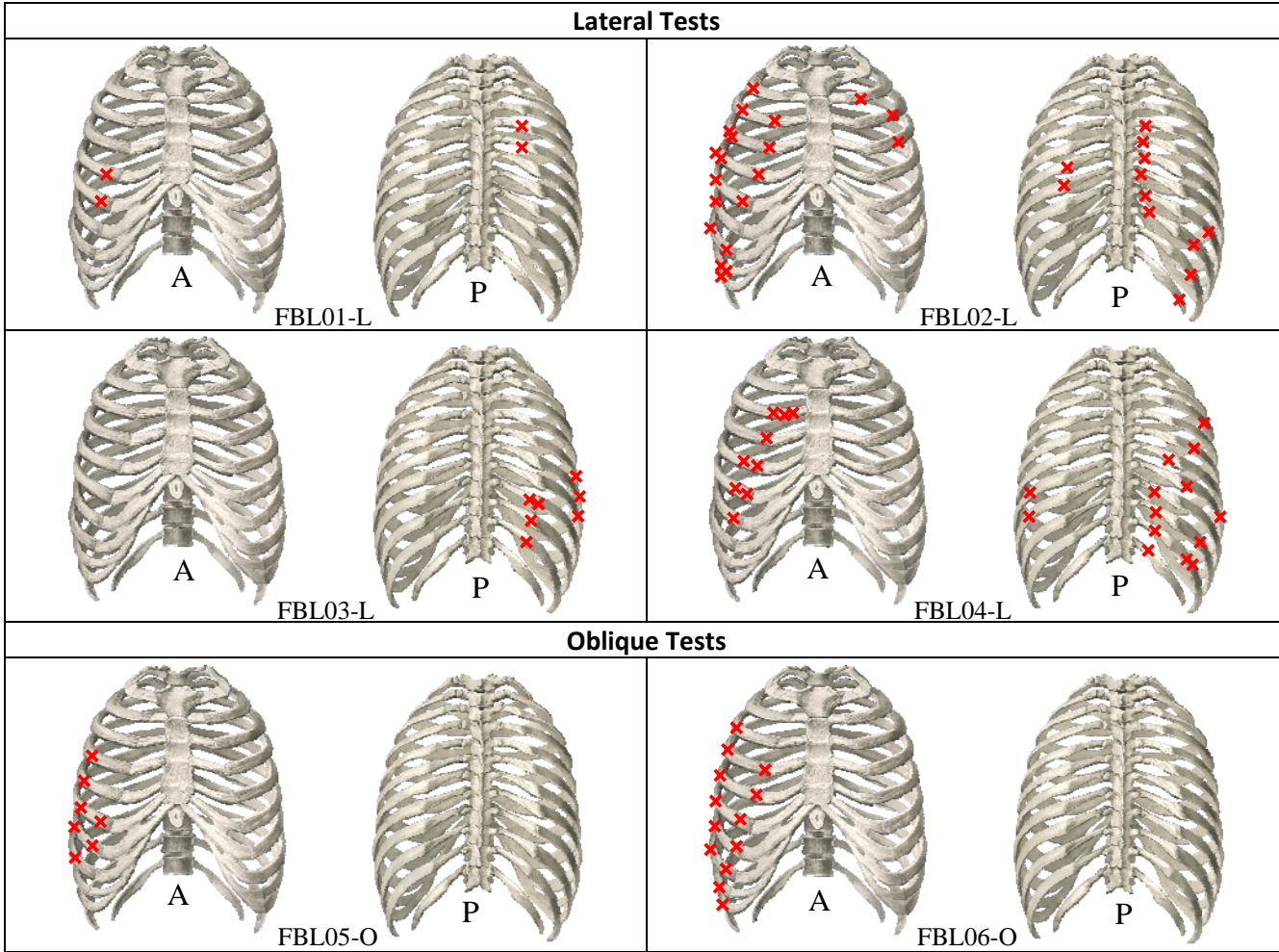
fractures.

Figure 3.1: Locations of Rib Fractures with Anterior and Posterior Views of the Thorax

3.2 Pressure

In some of the tests, the pressure sensors were not located exactly as desired. In some cases natural blockages in the arteries, such as plaque in the vessel prevented the instrumentation from being properly located.   In other cases, the pressure sensor location was incorrectly identified during two-dimensional fluoroscopy, such as in FBL01-L where it appeared the sensors were in the hepatic veins when the sensors were actually still in the right atrium. In three tests, the arterial instrumentation was inserted directly into the arch of the aorta since it was difficult to direct the sensors down into the descending aorta through the left common carotid artery.   For one test, test FBL05-O, there was limited space in the IVC between the heart and the hepatic veins so the sensors were placed in the IVC and the balloon was filled in the right atrium.

The issues with the internal instrumentation are summarized in Table 3.3. The tests highlighted in orange represent tests in which the pressure data seemed erroneous, likely due to lack of pressurization of the arterial side.   The pressure readings from these tests will not be included in our analysis. The tests highlighted in pink represent tests in which the sensors were not located within the hepatic veins. These tests will still be considered when analyzing the venous pressure and related variables since the sensors were still located within the venous vasculature, such as in the IVC or renal vein.

Table 3.3: Summary of Issues with Pressure Sensor Placement

Test	Venous	Arterial
FBL01-L	Pressure sensors in right atrium of the heart, not in hepatic vein	
FBL02-L		Natural blockage inferiorly in the descending aorta prevented inserting inferior instrumentation
FBL03-L		The inferior pressure sensor seemed to have either punctured the vessel wall or hit a natural blockage and could not be placed
FBL04-L	Pressure sensors in renal vein, not in hepatic vein	Pressure sensors inserted directly through arch of the aorta, Inferiorly, had to used string to tie off femoral artery because the foley balloon could not be inflated in the vessel without being punctured by plaque
FBL05-O	Pressure sensors in IVC, not in hepatic vein due to limited space between right atrium and hepatic veins	Pressure sensors inserted directly through arch of the aorta
FBL06-O	Pressure sensors were inserted very far into hepatic vein and were very close to the impactor face	Pressure sensors inserted directly through arch of the aorta

The change in vascular pressure was measured for each test and the change in liver tissue pressure was also measured for tests FBL05-O and FBL06-O. As an example, the plots of pressure in the descending aorta, inferior vena cava, hepatic vein, and liver tissue for test FBL06-O is shown in Figure 3.2. It should be kept in mind that the pressure readings are not an absolute value of the pressure but rather the change in pressure during the impact. The pressure sensor measurements were zeroed at 10 ms before time zero.
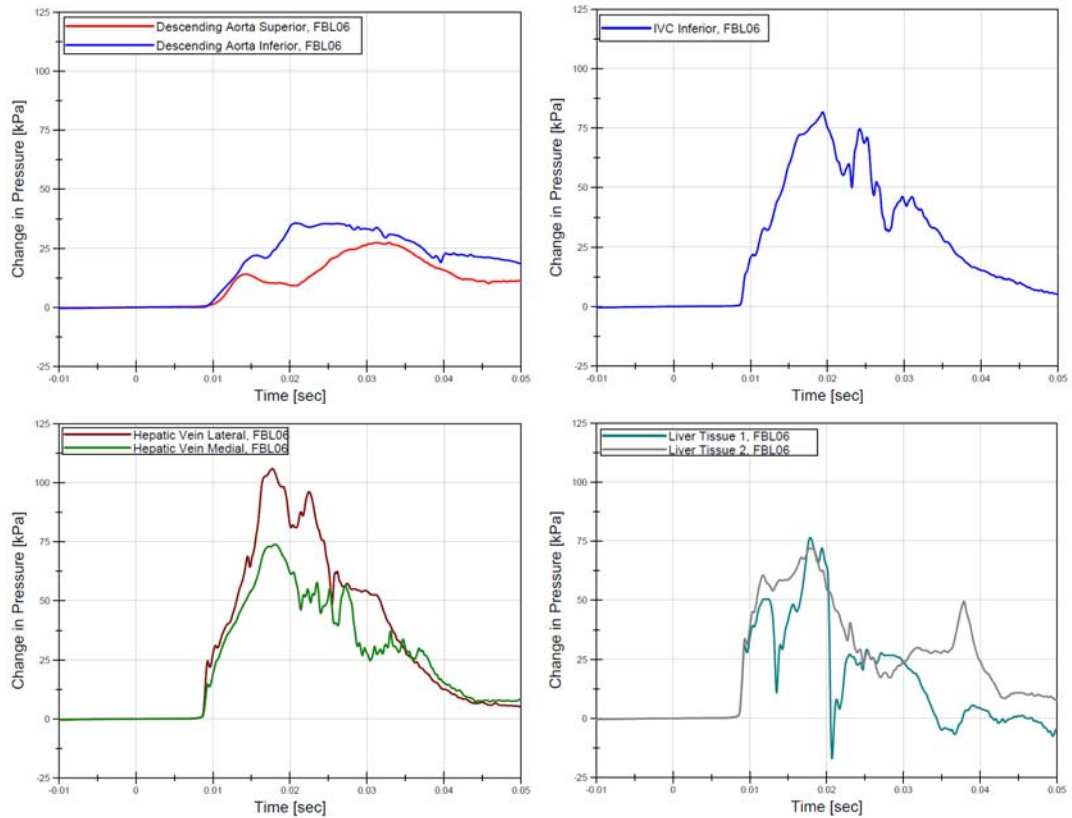
Figure 3.2: Example of Pressure Plots Obtained A- Arterial Pressure FBL06-O, B- Venous Pressure FBL06-O, C- Hepatic Vein Pressure FBL06-O, D- Liver Tissue Pressure FBL06-O

3.3 Relationship between Pressure and Sensor Distance

The distance between the center of the impact face and the pressure sensors had a statistically significant relationship to both the change in pressure (p=0.014, R^2 adjusted=0.265) and the rate of change of pressure in the venous vasculature (p<0.001, R^2 adjusted=0.516). The relationships are shown in Figure 3.3 and Figure 3.4. Other distance variables were also shown to be statistically significant predictors of P_{max} and $\dot{P}_{max}$ but this resultant was selected because it was statistically significant for both P_{max} and $\dot{P}_{max}$. The location of the sensors in the liver tissue was not measured so the liver tissue sensors are not included in this analysis.
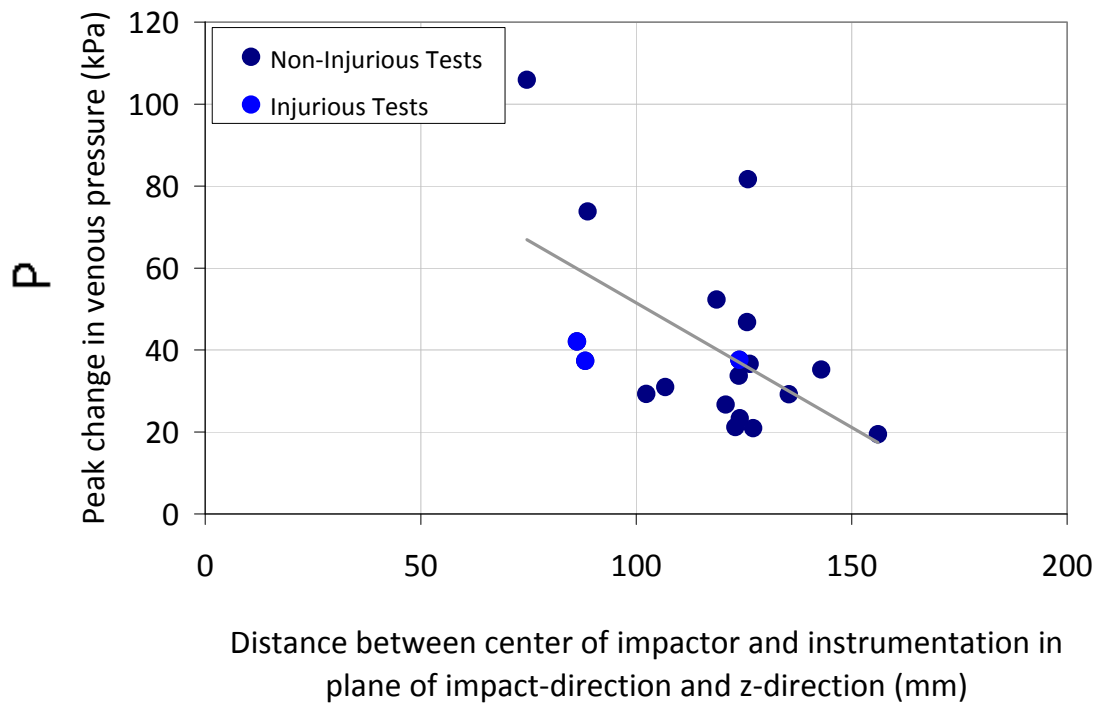
Figure 3.3: Pressure Change vs. Initial Location of Instrumentation
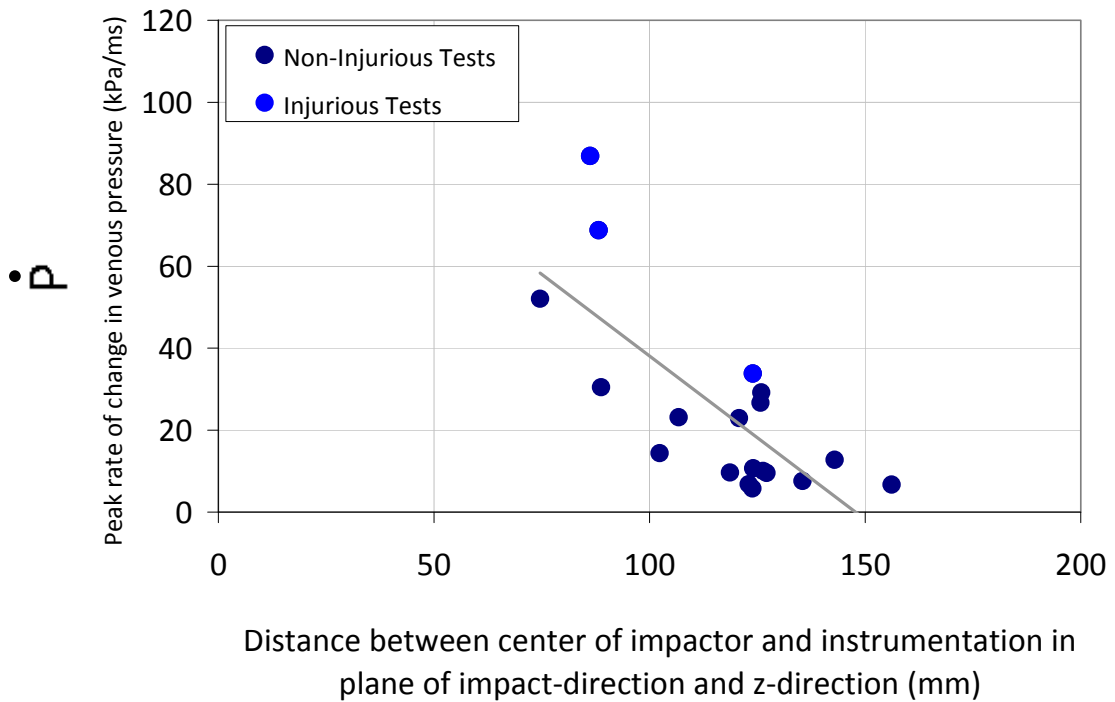
Figure 3.4: Rate of Pressure Change vs. Initial Location of Instrumentation

3.4 Pressure-related Variables

In addition to looking at the change in pressure, other pressure related variables were calculated for the pressure sensors in the venous vasculature, and the results are given Table 3.4. In the columns labeled AIS 2+ and AIS 3+, the number 0 indicates no AIS 2+ or AIS 3+ injury while the number 1 indicates presence of an AIS 2+ or AIS 3+ injury. The method of calculation is given in the data processing section. Test FBL03-L is highlighted in yellow since the test resulted in serious liver injury. The calculated pressure variables for the sensors in the liver tissue are given in Table 3.5.

Table 3.4: Pressure-Related Variables for the Venous Vasculature

Test	Sensor Location	P_{Max} (kPa)	$\dot{P}_{Max}$ (kPa/ms)	$\dot{P}_{Max}*P_{Max}$ (kPa^2/ms)	$[\dot{P}*P]_{Max}$ (kPa^2/ms)	Abdominal Injury	
						AIS 2+	AIS 3+
FBL01-L	Right Atrium, Medial	23.3	10.7	249	146	1	0
	Right Atrium, Lateral	29.3	14.4	421	145	1	0
	IVC Superior	33.7	5.7	194	119	1	0
	IVC Inferior	36.6	10.0	368	353	1	0
FBL02-L	Hepatic Vein, Medial	20.9	9.6	200	175	0	0
	Hepatic Vein, Lateral	21.2	6.8	144	123	0	0
	IVC Inferior	19.4	6.7	131	43	0	0
FBL03-L	Hepatic Vein, Medial	37.3	68.8	2567	1304	1	1
	Hepatic Vein, Lateral	42.1	86.9	3657	1777	1	1
	IVC Inferior	37.6	33.8	1270	343	1	1
FBL04-L	Renal Vein	30.9	23.1	715	278	0	0
	IVC Inferior	35.2	12.8	449	221	0	0
FBL05-O	IVC Superior 1	29.2	7.6	222	169	1	0
	IVC Superior 2	46.8	26.7	1248	1132	1	0
	IVC Superior 3	26.7	22.9	611	385	1	0
	IVC Inferior	52.3	9.7	505	369	1	0
FBL06-O	IVC Inferior	81.7	29.2	2383	826	1	0
	Hepatic Vein, Medial	73.8	30.4	2247	978	1	0
	Hepatic Vein, Lateral	105.9	52.1	5514	3521	1	0
Average		41.3	24.6	1215.4	653.0	-	-
Standard Deviation		± 22.8	± 22.5	± 1454	± 845	-	-

Table 3.5: Pressure-Related Variables for the Liver Tissue Sensors

Test	Sensor Location	P_{Max} (kPa)	$\dot{P}_{Max}$ (kPa/ms)	$\dot{P}_{Max}*P_{Max}$ (kPa^2/ms)	$[\dot{P}*P]_{Max}$ (kPa^2/ms)	Abdominal Injury	
						AIS 2+	AIS 3+
FBL05-O	Liver Tissue	81.8	67.2	5496	2315	1	0
FBL06-O	Liver Tissue 1	76.4	72.4	5536	1949	1	0
	Liver Tissue 2	72.0	65.2	4694	1689	1	0
Average		76.7	68.3	5242	1984	-	-
Standard Deviation		± 4.9	± 3.7	± 475.1	± 314.4	-	-

Binary logistic regression (α=0.05) was used to evaluate the risk of injury with respect to the pressure-related variables. All variables were analyzed for their relationship to AIS 2+ and AIS 3+ injuries by fitting the data to a risk function of the form:

(3.1)   Probability of AIS 2+ or AIS 3+ injury= $\dfrac{e^{(a+bx)}}{1+e^{(a+bx)}}$

where

      x= measured or calculated pressure-related variable

      a, b= model coefficients

      Statistical significance was assessed using the log-likelihood test.

      Table 3.6 gives a complete table of pressure related variables analyzed. In the analysis, the data point from the lateral, hepatic vein sensor in test FBL06-O was excluded because this point was an outlier because the sensor was located so far into the hepatic vein that it was likely in the tissue. This caused abnormally high values of pressure and the peak rate of change of pressure. The statistically significant factors are highlighted in green, with the darker green indicating variables for which the risk curves are plotted.   These models were selected because the log-likelihood test value of the model was higher and the gamma value was close to one. The model parameters for these models are given in Table 3.7. Plots of the injury risk functions are given in Figure 3.5 through Figure 3.8.

Table 3.6: Table of Relationships between Pressure Variables and AIS 2+ or AIS 3+ Injury

	AIS 2+ Abdominal Injury			AIS 3+ Abdominal Injury		
	Significance	Log Likelihood	Goodman-Kruskal Gamma	Significance	Log Likelihood	Goodman-Kruskal Gamma
P_{max}	p=0.009	-7.196	0.72	p=0.881	-8.099	0.44
$\dot{P}_{max}$	p=0.073	-9.033	0.51	p<0.001	0.00	1.00
$\dot{P}_{max}P_{max}$	p=0.031	-8.311	0.60	p=0.007	-4.482	0.91
$[\dot{P}*P]_{max}$	p=0.014	-7.644	0.60	p=0.017	-5.268	0.77

Table 3.7: Binary Logistic Regression Injury Risk Models for Selected Pressure Related Variables

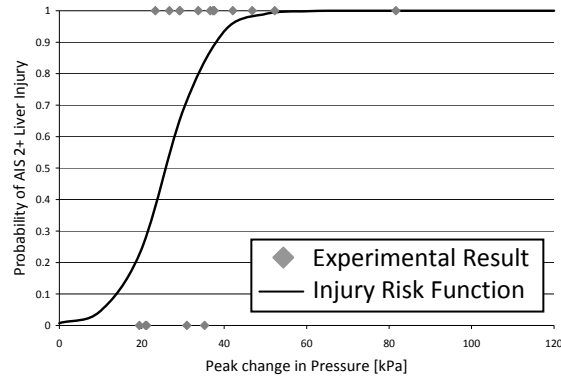|	Model Parameters		Significance	Log Likelihood	Goodman-Kruskal Gamma
	a	b			
AIS 2+ Injury vs. P_{max}	-4.928	0.190	p=0.009	-7.196	0.72
AIS 3+ Injury vs. $\dot{P}_{max}$	-461.71	14.377	P<0.001	0.000	1.00
AIS 3+ Injury vs. $P_{max} \cdot \dot{P}_{max}$	-4.335	0.00183	p=0.007	-4.482	0.91
AIS 3+ Injury vs. $[P \cdot \dot{P}]_{max}$	-3.826	0.00316	p=0.017	-5.268	0.77

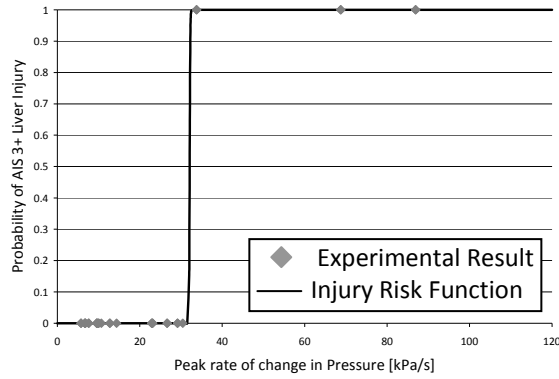Figure 3.5: AIS 2+ Injury Risk vs. P_{max}

Figure 3.6: AIS 3+ Injury Risk vs. $\dot{P}_{max}$

Figure 3.7: AIS 3+ Injury Risk vs. $P_{max} * \dot{P}_{max}$
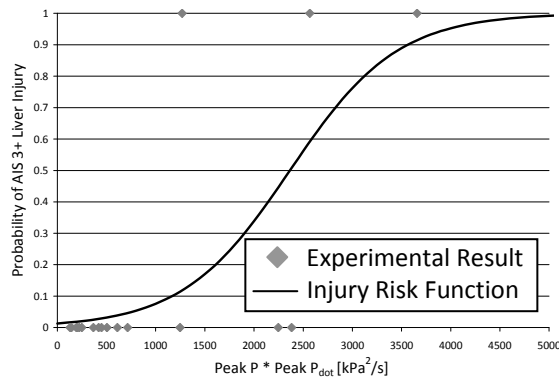

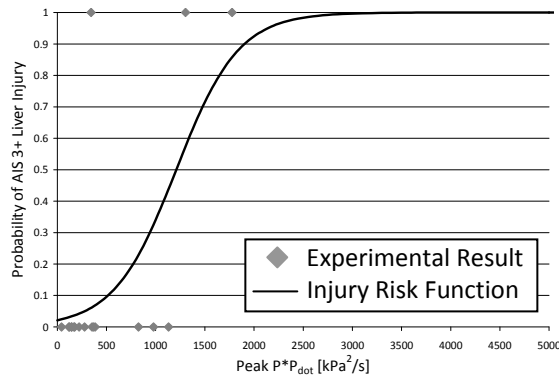Figure 3.8: AIS 3+ Injury Risk vs. $[P * \dot{P}]_{max}$

3.5 Pressure vs. Compression

The pressure-compression relationship for the lateral and oblique tests is shown in

Figure 3.9. The pressure and compression data were plotted from time=0 to time=0.04 s. This

time period was selected since the maximum compression occurs between 0.0235 and 0.0258 s.
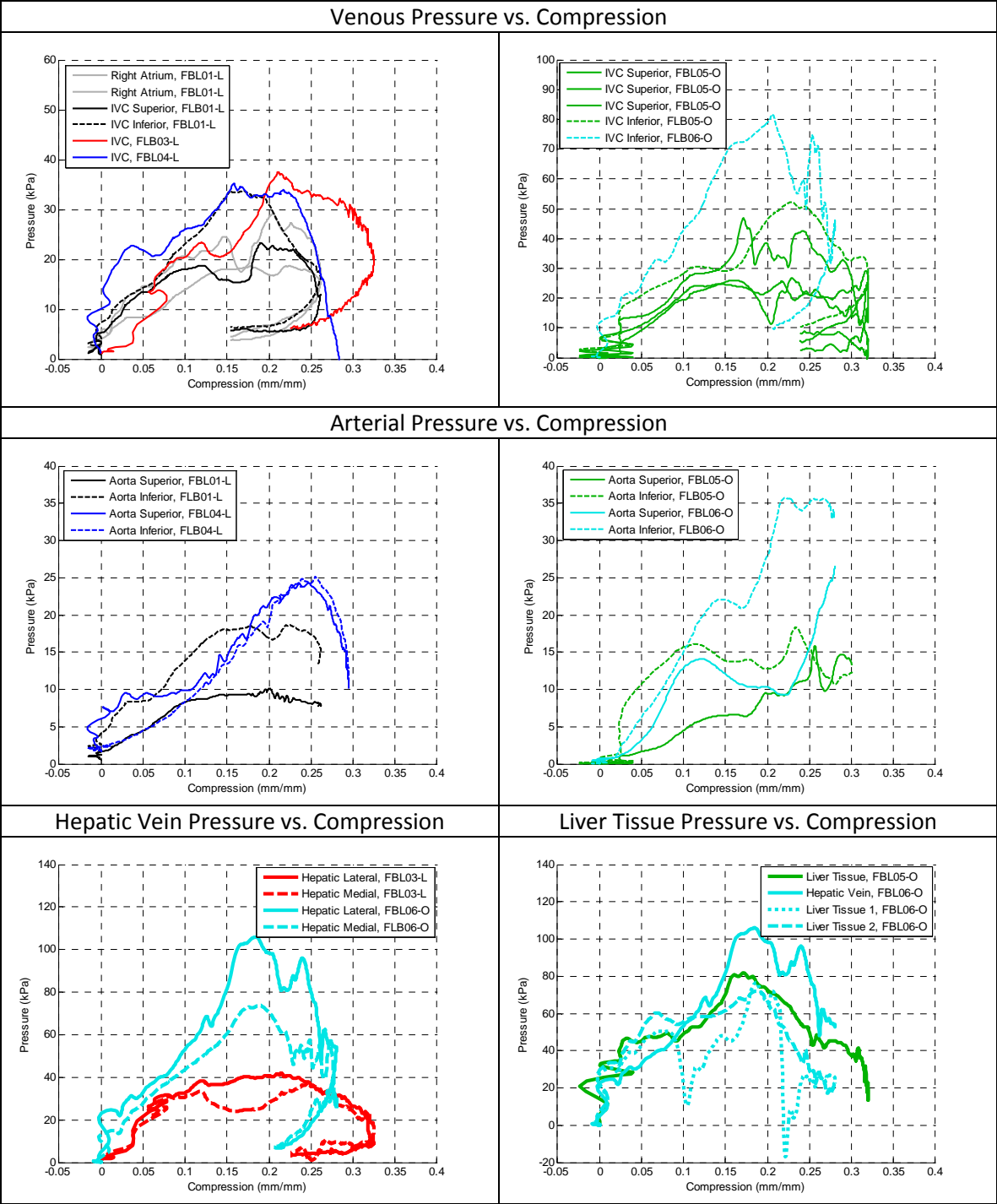
48

Figure 3.9: Pressure vs. Compression

3.6 Other Biomechanical Variables

A table of non-normalized biomechanical variables is given in Table 3.8. The complete

list of the effective masses and scaling factors is given in Table 3.9. The normalized

biomechanical variables are given in Table 3.10.

Table 3.8: Non-Normalized Biomechanical Variables

	Variable	Peak Ram Force (F)	Displacement (d)	Compression (c)	Time max displacement (T_d)	VC_{max}	$V_{max}C_{max}$	$\dot{F}C$	Liver Injury AIS Rating
	Units	N	mm	unitless	s	m/s	m/s	N/ms	
Lateral Tests	FBL01-L	5128.0	78	0.26	0.0235	1.03	1.9	13.8	2
	FBL02-L	3903.0	-	-	0.0248	-	-	-	0
	FBL03-L	4782.5	95	0.32	0.0249	1.72	2.3	85.4	4
	FBL04-L	4782.2	88	0.30	0.0258	1.30	2.1	26.3	0
	Average	4648.9	86.9	0.29	0.0247	1.35	2.1	41.8	-
	Standard Deviation	$\pm$523.3	$\pm$8.8	$\pm$0.03	$\pm$0.0010	$\pm$0.35	$\pm$0.2	$\pm$38.3	-
Oblique Tests	FBL05-O	4148.2	92	0.32	0.0253	1.07	2.3	29.8	2
	FBL06-O	5423.5	88	0.28	0.0254	1.07	2.0	32.8	2
	Average	4785.9	89.9	0.30	0.0254	1.07	2.1	31.3	-
	Standard Deviation	$\pm$901.8	$\pm$3.4	$\pm$0.03	$\pm$0.0001	$\pm$0.003	$\pm$0.2	$\pm$2.2	-
All Tests	Average	4694.6	88.1	0.30	0.0250	1.24	2.1	37.6	-
	Standard Deviation	$\pm$576.1	$\pm$6.7	$\pm$0.03	$\pm$0.0009	$\pm$0.29	$\pm$0.2	$\pm$27.7	-

Table 3.9: Normalization Factors

	M_{eff} (kg)	R_m	R_k	R_d	R_t	R_f
FBL01-L	31.19	1.15	1.18	1.02	1.04	1.20
FBL02-L	22.04	1.63	0.95	1.44	1.44	1.37
FBL03-L	40.50	0.89	1.29	0.85	0.84	1.10
FBL04-L	31.07	1.15	1.28	1.02	1.02	1.31
FBL05-O	20.56	1.43	1.16	1.25	1.26	1.45
FBL06-O	32.08	0.92	1.13	0.88	0.88	1.00

Table 3.10: Normalized Biomechanical Variables

	Variable	Peak Ram Force (F)	Displacement (d)	Time max compression (T_d)	$\dot{F}C$
	Units	N	mm	s	N/ms
	Factor	R_f	R_d	R_t	R_f/R_t
Lateral Tests	FBL01-L	6169.1	80	0.02756	16.0
	FBL02-L	5335.8	-	0.03561	-
	FBL03-L	5255.1	81	0.03219	110.4
	FBL04-L	6242.2	89	0.03292	33.6
	Average	5750.6	83.3	0.03207	53.3
	Standard Deviation	$\pm$527.4	$\pm$5.3	$\pm$0.00335	$\pm$50.2
Oblique Tests	FBL05-O	6016.4	115	0.02943	34.4
	FBL06-O	5417.2	77	0.02878	37.2
	Average	5716.8	96.2	0.02911	35.8
	Standard Deviation	$\pm$423.7	$\pm$26.8	$\pm$0.00046	$\pm$2.0
All Tests	Average	5739.3	88.4	0.03108	46.3
	Standard Deviation	$\pm$450.6	$\pm$15.6	$\pm$0.00302	$\pm$36.8

3.7 Chestband Analysis

      The output of the chestband analysis program is the time history of the movement of

the gages in the x- and y-planes, assuming that the gage at the spine is stationary. Plots of the

chestband position at various points in time for each test are given in Figure 3.10 through Figure

3.14. The purple plot represents the initial position of the chestband while the blue plot

represents the position at the time of maximum compression. Test FBL02-L did not have

chestband data because some of the chestband data channels were cut off due to an issue with
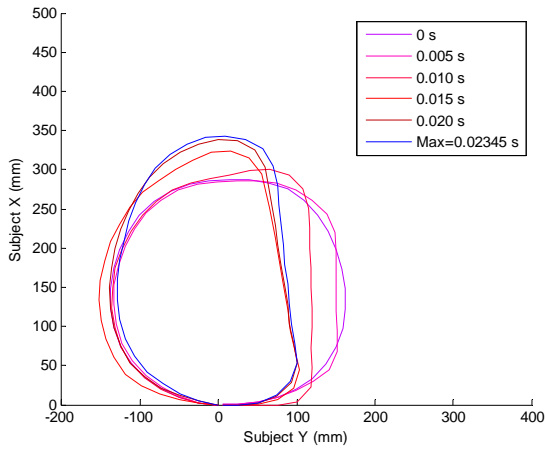
the data acquisition system.
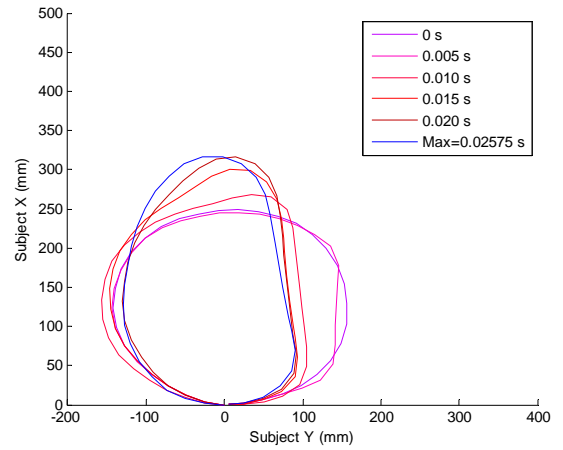
Figure 3.10: Chestband Movement, FBL01-L

Figure 3.12: Chestband Movement, FBL04-L
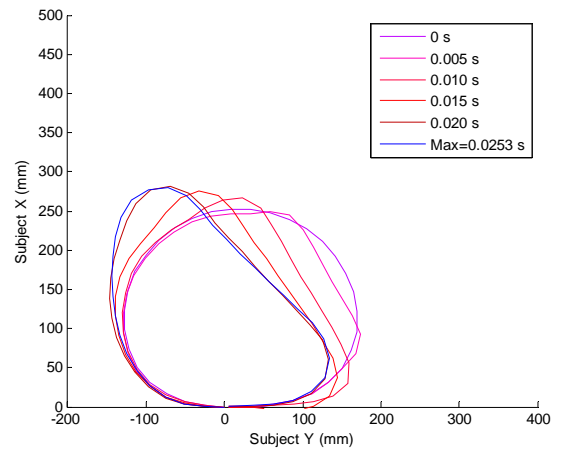
No Chestband data for FBL02-L

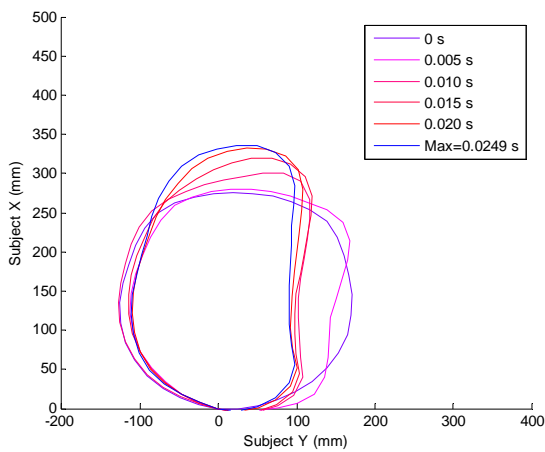
Figure 3.13: Chestband Movement, FLB05-O
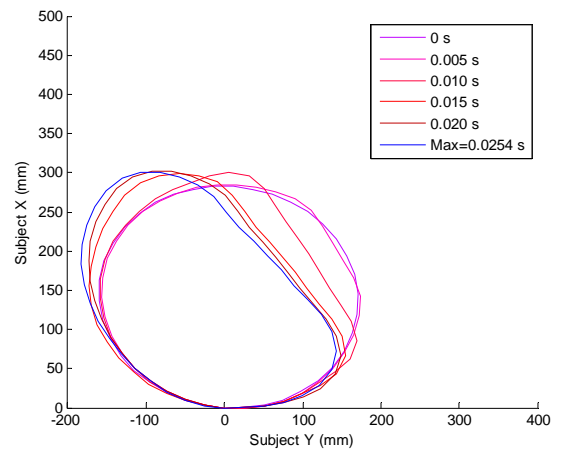

Figure 3.11: Chestband Movement, FBL03-L

Figure 3.14: Chestband Movement, FBL06-O

3.8 Time Histories of Force and Displacement

The applied force was calculated from the ram acceleration on the mass of the ram. The plot of the non-normalized force-time history is given in Figure 3.15. The plot of the normalized force-time history is shown in Figure 3.16. The lateral and oblique tests are plotted separately.
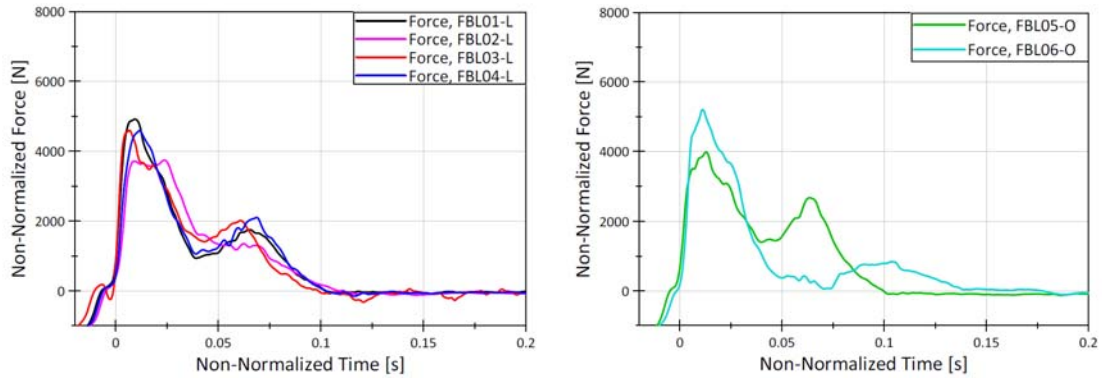

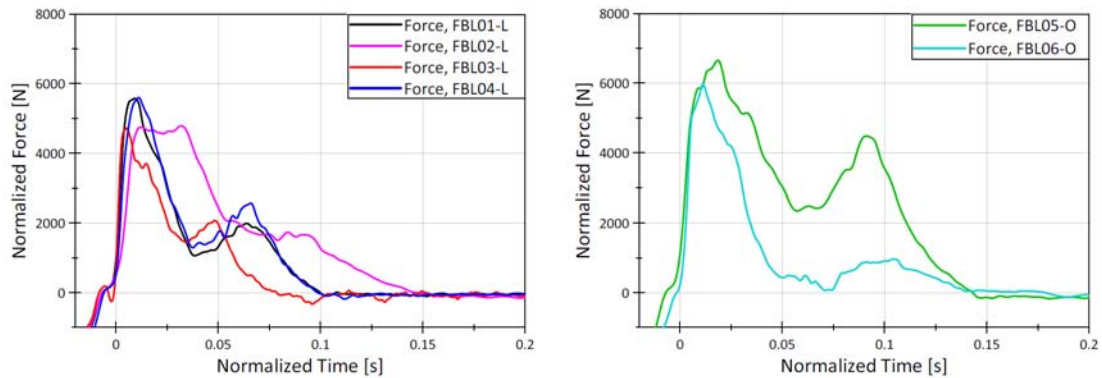Figure 3.15: Non-Normalized Force-Time History

Figure 3.16: Normalized Force-Time History

The displacement was calculated using the chestband data. The time histories of the non-normalized and normalized displacements are shown in Figure 3.17 and Figure 3.18. Again, the lateral and oblique tests are plotted separately.
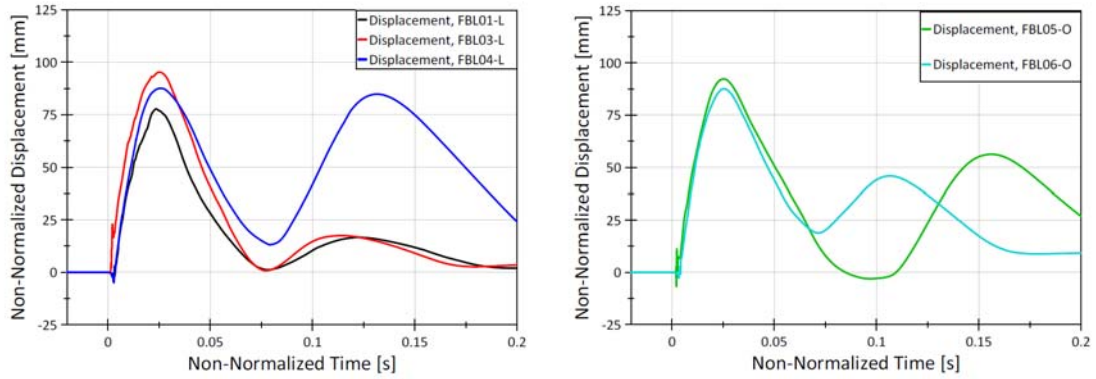
Figure 3.17: Non-Normalized Displacement-Time History
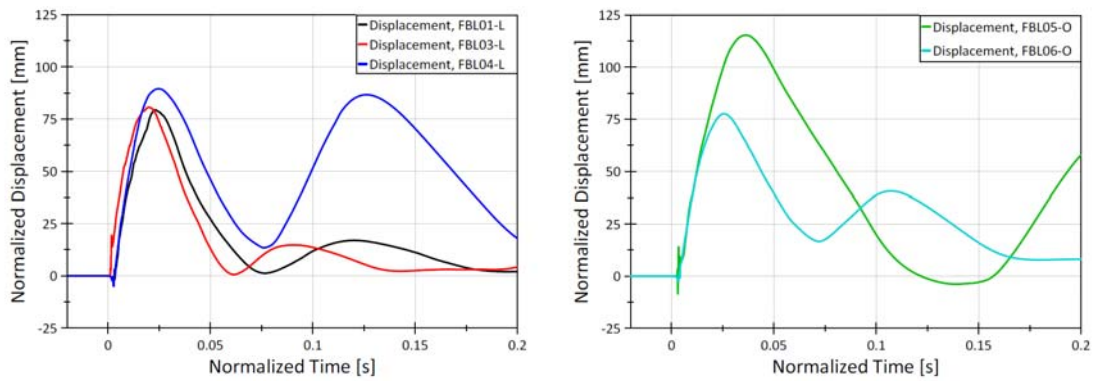
Figure 3.18: Normalized Displacement-Time History

3.9 Force-Compression and Force-Displacement

The response of the thoraco-abdominal region may be characterized by force-displacement and force-compression plots. Plots were created for the non-normalized data sets and for the data sets with the displacement and the force normalized for the time period from 0 s to 0.04 s. These are shown in Figure 3.19 and Figure 3.20.

57

Figure 3.19: Force vs. Displacement Histories. A- Non-Normalized Lateral Tests, B- Non- Normalized Oblique Tests, C- Normalized Lateral Tests, D- Normalized Oblique Tests

Figure 3.20: Force vs. Compression Histories. A- Non-Normalized Lateral Tests, B- Non- Normalized Oblique Tests, C- Normalized Lateral Tests, D- Normalized Oblique Tests

Chapter 4: Discussion

4.1 Injuries

This test series resulted in one test with serious (AIS 3+) liver injury (FBL03-L) and three

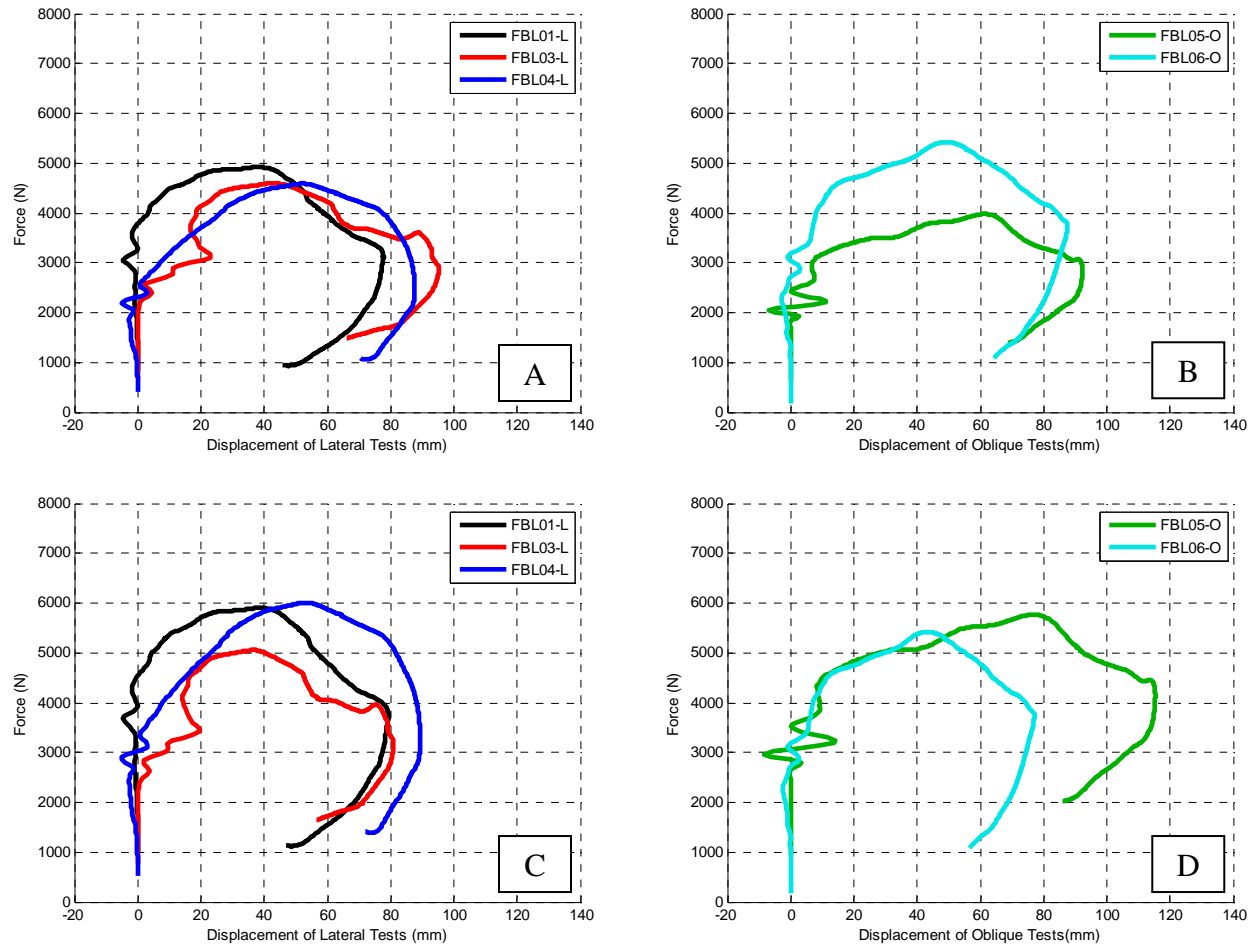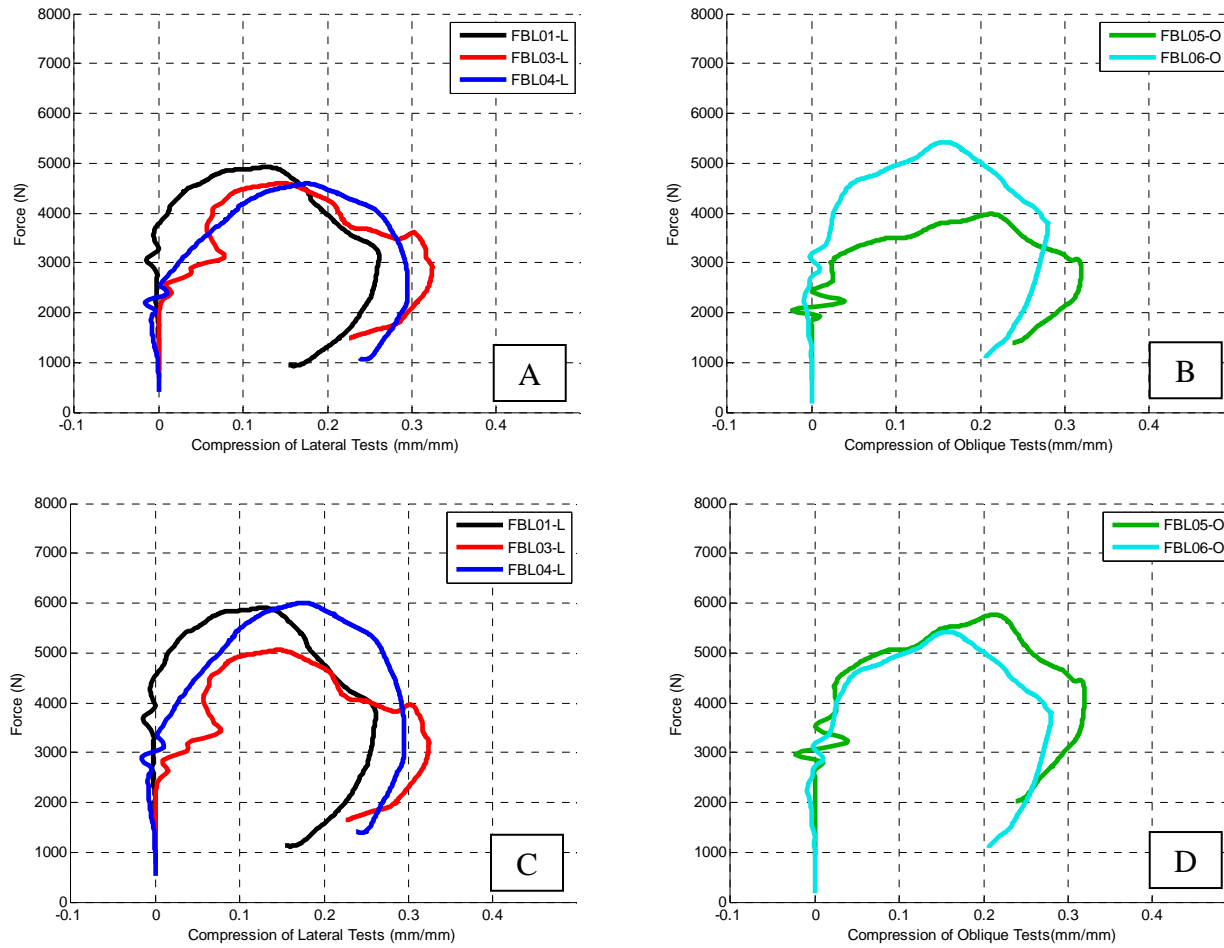tests with laceration (AIS 2) injuries to the liver (FBL01-L, FBL05-O and FBL06-O). The lacerations

did not appear to be the result of rib fractures since there were no displaced rib fractures

corresponding to the laceration locations.   However, fractured ribs allowed for more

compression of the liver and more force to be transmitted to the liver which would increase the

stress to the capsule. Additionally some of the lacerations appeared to correspond to the edge

of the impactor, especially in tests FBL01-L and FBL06-O. The liver tissue interacting with the

plate would be quickly accelerated at the time of impact. The liver tissue not interacting with

the plate would tend to remain stationary until pulled by the liver tissue being moved by the

plate. This would increase the stress in the capsule at this point and could cause lacerations to

the liver.

Since the liver is located directly behind the rib cage, it is difficult to load the liver

without also loading the rib cage. In studies of MVCs, the presence of rib fractures has been

found to increase the risk of liver injuries (Lee, 1990, Shweiki, 2001).   All tests resulted in at

least two fractured ribs. While all tests were performed at the same velocity, the number of

skeletal injuries varied greatly. A contributing factor to the variation in injuries was likely the

variation in bone mineral density. Subject FBL02-L and Subject FBL04-L had the lowest bone

mineral densities with t-scores of -1.5 and -1.6, respectively. These subjects both had extensive

rib fractures. These two subjects were also the only two subjects to have left hemisphere rib

fractures. Bone mineral density is not the only cause of variation in the number of rib fractures.

Variation in the composition of the bones, the shape of the thorax, the curvature and geometry

of the ribs, and kinematics of the thorax may cause differences in the number and patterns of

rib fractures.

The rib fractures tended to be located in two straight line patterns along the thorax, as

illustrated in Figure 4.1.   The patterns tended to be on the anterior and posterior thorax for the

lateral testing and on the anterior thorax for the oblique testing. The pattern was a result of the

blunt plate loading that created symmetric failures of the ribs. The occurrence of rib fractures in

straight line patterns can be attributed that the fact that the rib structure is weakened by a

fracture which then increases the loading on the nearby ribs.

Anterior   Posterior
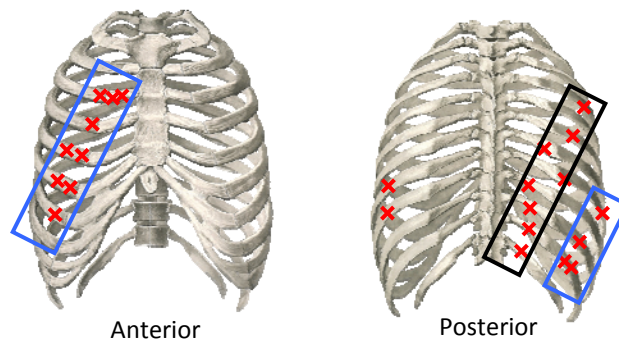
Figure 4.1: Schematic of Rib Fractures in FBL04-L

The liver injuries obtained in this testing were compared to those obtained in real world

automobile accidents from the CIREN database. The results are summarized in Table 4.1. The

patterns observed from the laboratory setup were similar to the injury patterns of occupants of

motor vehicle crash.

61

Table 4.1: Liver Injury Images from the CIREN Database Compared to Images from Test Series

Ciren Image	Description	Test Image
	Superficial laceration of the capsule	FBL01-L
	Serious parenchymal disruption	FBL03-L
	Multiple superficial parallel lacerations ("bear claw" lacerations)	FBL06-O
	Parenchymal disruption	FBL06-O
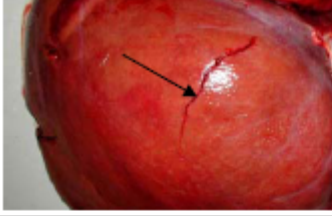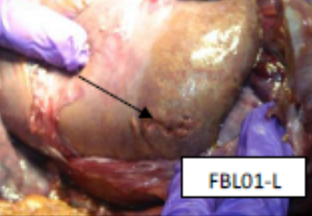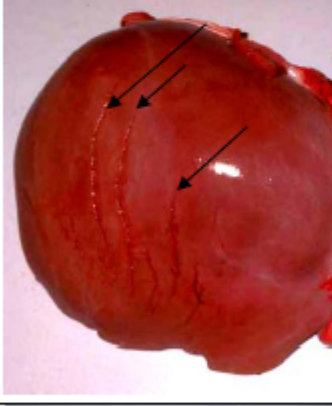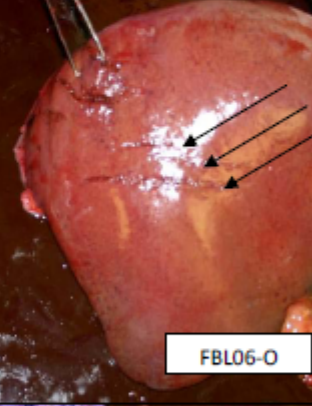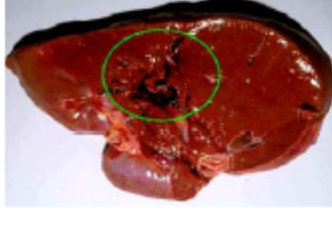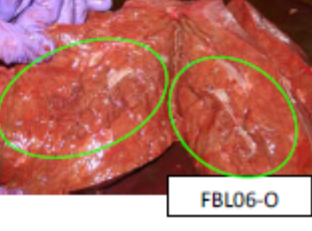
4.2 Pressure

For the pressure-related variables, it was decided to focus on the venous pressures, including sensors located in the hepatic veins, IVC, renal veins, and right atrium. There were more issues with the arterial blockages that resulted in unusable data points and when considering the limited number of data points, no strong correlations were shown between the arterial pressure or related variables and injury. One explanation for stronger relationships

between venous pressure-related variables and injury is the IVC and hepatic veins are located on the right side of the vertebral column. The descending aorta is on the left side of the vertebral column, opposite the loading. The further distance may reduce the response in the arterial vessels. Additionally, venous vessel walls are thinner than the artery walls. The venous vasculature, especially the hepatic veins, may be subject to deformation by the surrounding liver tissue thus resulting in more pressure response in the veins due to impact. The accuracy of arterial pressure measurements could also be adversely affected by the presence of plaque in the vessels which could constrict the vessels or cause abnormal fluid flow. One important observation about the arterial pressure is that the peak pressures in the venous vessels occur earlier than the peak arterial pressures. This is explained by the facts that the venous pressure sensors are closer to the impact point than the arterial pressure sensors.

The initial distance of the instrumentation from the impact point and the peak venous pressure change was found to be significant (R^2 adjusted=0.265, p=0.014), as was the distance compared to the peak rate of pressure change (R^2 adjusted=0.516, p<0.001). The instrumentation that was closer to the right lateral side tended to measure higher pressure changes and higher rates of pressure change. This is important to note because there was significant variation in initial distances of the sensors so differences in P_{max} and $\dot{P}_{max}$ may be partially explained by differences in variation in locations. In Figure 3.3, the pressures measured in the injurious tests are similar to those in the non-injurious tests, when considering the lateral and oblique tests. However, in Figure 3.4, the peak rate of pressure change in the injurious tests is above the trend line for all the data points. Although $\dot{P}_{max}$ shows a dependence on location, the magnitudes of $\dot{P}_{max}$ tend to be higher for injurious test.

In looking at the table of pressure-related biomechanical variables, a few things should be noted. First, test FBL03-L resulted in serious abdominal injury and had the highest pressure measured on the venous side of all the lateral tests. However, as noted earlier, the variation in pressure sensor readings could be affected by the location of the sensor relative to the impactor. Both oblique tests, FBL05-O and FBL06-O, resulted in higher peak pressure changes than FBL03-L. This could be a result of more compression of the liver between the impactor and the spine during oblique impacts as a result of the relative location of the sensors to the impactor.

Second, the peak rate of pressure change seemed to be the strongest predictor of liver injury. Although FBL03-L did not have the highest pressure of all the tests, lateral and oblique tests included, it did have the highest $\dot{P}_{max}$ value. If the data point for the lateral hepatic vein in FBL06-O is excluded, FBL03-L has the three highest values of $\dot{P}$ for all the tests. Combinations of $\dot{P}$ and P were also calculated. These also appeared to be strong predictors of injury with high values for the injurious test.

Binary logistic regressions were performed for the pressure-related variables. In the analyses, the point from the hepatic vein in test FBL06-O was excluded. The reason for exclusion was the sensor was advanced as far as possible to where the hepatic vein diameter would have been quite small. It is conceivable that the sensor was surrounded by the vein walls, not fluid, as the other sensors were. For abdominal injuries, P_{max} was found to be a strong predictor of AIS 2+ injuries (p=0.009, γ=0.72). $\dot{P}_{max}$ was found to be a strong predictor of AIS 3+ injuries (p<0.001, γ=1.00). A gamma value of one indicates that $\dot{P}_{max}$ for the injurious tests was higher than for every non-injurious test. $\dot{P}_{max}P_{max}$ and $[\dot{P}*P]_{max}$ are also significant predictors of AIS 3+ injury (p=0.007, γ=0.91 and p=0.017, γ=0.77) for our data set.

One limitation of this analysis is that there were a limited number of tests being considered in this analysis. When considering AIS 2+ abdominal injuries, only two tests did not have injury. When AIS 3+ abdominal injuries were considered, only one test resulted in serious liver injury. Hopefully these relationships will be improved with more data points from in situ measurements of the pressure in the venous vasculature.

4.3 Pressure vs. Compression

When plotting the pressure in the arteries and IVC versus compression, shown in Figure 3.9, the lateral and oblique tests were plotted separately since the loading of the thorax is different in each case. However, only three tests had the hepatic vein sensors in the proper location. Since there was no chestband data in test FBL02-L, the lateral and oblique tests were plotted together for the pressure-compression characterization. The lateral tests generally saw a similar trend for the slope of the arterial and IVC pressure, especially up to compression levels of 15%. The oblique tests, however, had more varying slopes, including some difference of the slopes of the aorta superior and inferior sensors in the same vessel in test FBL05-O. This could be a result of the pressure sensor being located against the vessel wall or the result of plaque in the vessel.

For the liver tissue plots, the sensor from the lateral hepatic vein in test FBL06-O was included with the liver tissue sensors since the force-compression slope closely matches the liver tissue sensors and the sensor was nearly into the liver tissue at the end of the vein.

It is difficult to establish average responses of the pressure vs. compression curves. However, it is important to note that the peak pressure and the peak compression did not occur at the same time. The subjects generally saw the peak in pressure prior to the peak compression of the entire thorax. One explanation for this is that maximum compression of the

liver may occur prior to the maximum compression of the entire thorax. If it were possible to measure the compression of the liver, a stronger relationship might be found between pressure and compression. It also should be noted that the subjects with fewer rib fractures tended to have decompression of the thorax earlier since the rib cage would have an elastic response if there were not extensive rib fractures.

4.4 Comparison of Rate of Change of Pressure and KVC

An interesting result of the data analysis shows that a strong linear correlation exists between $\dot{F}C_{max}$ and $\dot{P}_{max}$ for the sensors in the hepatic vein or in the IVC near the hepatic veins (R^2 adjusted=0.635, p<0.001). This relationship is plotted in Figure 4.2. The force and the compression are both variables that are measured external to the body while the pressure is measured internally. The relationship between these two is significant because external variables are more difficult to measure in ATDs. If there is a relationship between an external variable and an internal variable, it may make assessing abdominal injury risk in ATDs easier.
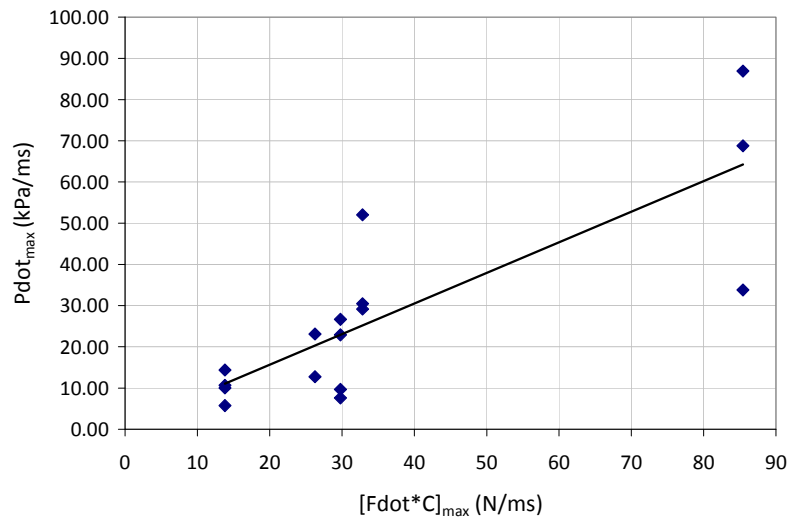
Figure 4.2: Peak Rate of Pressure Change vs. Peak KVC

However, since $\dot{P}_{max}$ showed a decreasing trend with increasing distance of the instrumentation from the impactor face, the effect of distance should be considered. To do this, the measured value of $\dot{P}_{max}$ was normalized by the value of $\dot{P}_{max}$ predicted using distance by the relationship between distance and $\dot{P}_{max}$. This gave a ratio of how many times greater the measured value of $\dot{P}_{max}$ was than what was expected for the given linear distance. When accounting for the distance from the impactor face, there still exists a positive correlation between peak rate of pressure increase and KVC (R^2 adjusted=0.600, p<0.001), shown in Figure 4.3.
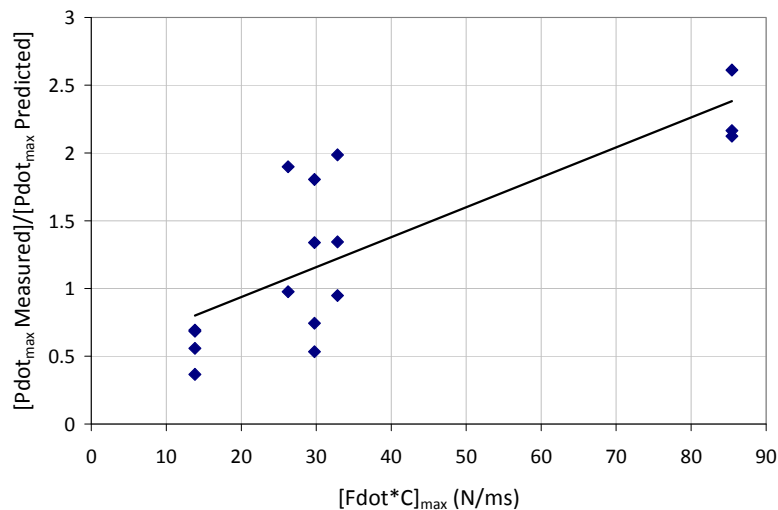
Figure 4.3: Normalized Peak $\dot{P}$ vs. KVC

The KVC was proposed as a measurement of how directly an abdominal organ was loaded. Since the abdominal organs have significant mobility, whether the organs displace out of the line of loading influences if injury is obtained or not. The movement of the organ out of the path of the loading is influenced by the speed of the impact and the directness of the load. In a slow impact, the organ can slide out of the way but in high speed impacts, the inertia of the organ prevents the organ from moving out of the line of the impact. Additionally, the closer the

impact to the organ's center of mass, the less likely the organ is to move out of the way. However, if the organ is loaded not through the center, the organ is more likely to more out of the way. Thus, the plots in Figure 4.2 and Figure 4.3 show that the rate of change of pressure may also measure how directly the abdomen was loaded.

An analogy to this behavior is popping a balloon. Popping a balloon is most likely if you quickly apply the load to the balloon and if you apply the load to the middle of the balloon. If you stomp on the side of the balloon, the side you step on will deform but most likely the balloon will simply move out of the way. If you step on the balloon slowly, the balloon is less likely to reach the critical stress and burst. Liver injuries are most likely to occur when the liver is loaded quickly and when the liver does not move out of the way. The rate of change of pressure is an indication of both how directly the liver is being loaded and how quickly the liver is being loaded.

It is interesting to note that the in FBL03-L where a serious liver injury was obtained, the cross-sectional area of the liver at the center of the impact plate was large, as shown in Figure 4.4. The center of the ram in the CT images was identified by the bony landmarks. This would indicate that in this test, the loading was fairly direct. However, in other tests, such as FBL01-L, the cross sectional area of the liver at the center of the impact plate was much smaller. This may explain the high value of $\dot{P}_{max}$ and $\dot{F}C_{max}$ in test FBL03-L since the organ was more directly loaded.
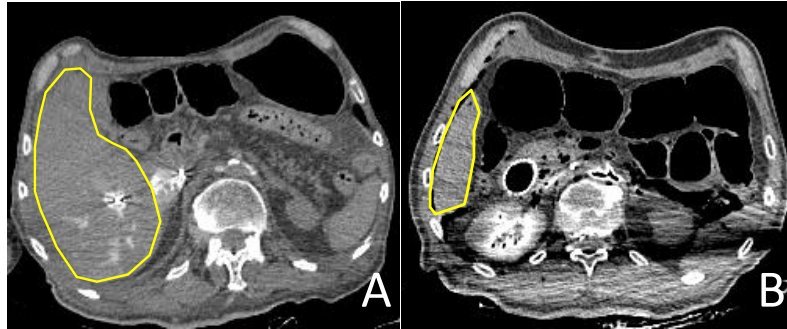
Figure 4.4: Comparison of Cross Sections at the Center of the Impact Face in FBL03-L (A) and FBL01-L (B)

4.5 Comparison to Ex Vivo Testing

The full body test results were compared to the *ex vivo* human liver testing was performed by Sparks et al. (2007). In both the full body testing and in the *ex vivo* testing, the pressure was found to be dependent on the location relative to the impactor. Comparing the measured vascular pressure, in the *ex vivo* testing it was found that a peak vascular pressure of 46.0 kPa corresponded to a 50% risk of serious injury.   For the lateral tests in the full body tests, the only subject that obtained serious liver injury had peak changes in the venous pressure ranging from 37.3 to 42.1 kPa while no other tests saw peak pressure changes higher than 36.6 kPa. The oblique tests were not included in this analysis because the peak pressures were significantly higher and they were not analyzed independently because no serious liver injuries resulted from the oblique testing. More test points are needed for full analysis of the oblique tests.

The *ex vivo* tests also found values for a 50% risk of serious injury related to the rate of change of pressure. These variables are compared to the full body results from the binary logistic regression of the vascular pressure in Table 4.2.

69

Table 4.2: Comparison of Values Predicting 50% Risk of AIS 3+ Injury *Ex vivo* and *In situ*

Variable	*Ex vivo* Testing (Sparks, 2007)	Current, *In situ* Testing
$\dot{P}_{max}$	27.5 kPa/ms	32.1 kPa/ms
$\dot{P}_{max}*P_{max}$	1370 kPa^2/ms	2366 kPa^2/ms
$[\dot{P}*P]_{max}$	1100 kPa^2/ms	1209 kPa^2/ms

It should be noted that the *ex vivo* testing used the tissue pressure to predict injury

while the *in situ* testing used vascular pressure. However, the Sparks study reported a

relationship between the tissue and location-corrected vascular pressures for the *ex vivo* testing

so it is felt that this is an acceptable comparison. The liver tissue pressure measurements were

excluded from the *in situ* analysis because it was only measured in two oblique tests, neither of

which resulted in serious injury. Therefore, it was not possible to correlate liver tissue pressure

to injury for the *in situ* testing. There is some variation between the *ex vivo* and *in situ* testing in

the values of the thresholds, especially for the $\dot{P}_{max}P_{max}$ value. Since the magnitudes of $\dot{P}_{max}$ were

similar in both test conditions, this indicates that the general trend was that the magnitude of

pressure change was higher for the injurious in situ testing than for the injurious ex vivo testing.

This could be a result of the different boundary conditions or the different direction of loading.

In spite of some differences in the value predicting a 50% risk of abdominal injury, both studies

found a correlation between injury and these pressure-related variables. This is a promising

direction to pursue in using pressure to predict injury.

The *ex vivo* testing also found that VC_{max} and $V_{max}C_{max}$ were predictors of serious injury,

with values of 0.69 and 0.82 m/s respectively corresponding to a 50% risk of injury. For the *in*

situ testing, all the values of the VC_{max} and $V_{max}C_{max}$ were above 0.69 and 0.82 m/s, respectively.

In the *ex vivo* testing, the velocity and compression were only related to the isolated liver. However, in the *in situ* testing, the rib cage and other abdominal organs are also interacting with the liver which changes the velocity and compression. Although VC_{max} and $V_{max}C_{max}$ were good predictors in the ex vivo testing, the values of these predictors are not comparable to the VC_{max} and $V_{max}C_{max}$ obtained in *in situ* testing.

4.6 Force, Velocity, and Compression-related Biomechanical Variables

Table 3.8 reports the non-normalized biomechanical variables. The force for the female subjects, FBL02-L and FBL05-O, was lower than the force for the male subjects. This can be attributed to the fact that the subjects weigh less and therefore provide less resistance to the movement of the ram. The female subjects also have more subcutaneous tissue laterally which would dissipate the energy. As for displacement and compression, the subject that sustained serious liver injury had the highest displacement and the highest compression of all the tests.

Using compression, other biomechanical variables were calculated including VC_{max}, $V_{max}C_{max}$, and $\dot{F}C_{max}$. All of these variables have been used to predict abdominal injury in previous research. For the test with serious liver injury, FBL03-L, the value of VC_{max} was found to be 1.72 m/s, the highest of all the tests. This value is lower than the reported VC_{max} of 1.98 m/s corresponding to 25% risk of AIS 4+ injury for lateral impacts to cadavers (Viano, 1989). For test FBL03-L, the abdominal injury criterion, $V_{max}C_{max}$, was found to be 2.28 m/s. However, test FBL05-O, where the subject only sustained a minor injury, had a value of 2.29 m/s. Abdominal injury criteria may not be a good discriminator when the nominal test velocity is the same for all subjects.

Finally, FBL03-L resulted in the highest value for the kinetic analog to the viscous criterion (KVC), $\dot{F}C_{max}$, of all the tests . Kent et al. (2008) reported that for swine with a fixed

71

back subject to belt loading, a $\dot{F}C_{max}$ of 0.528 N/ms predicted an AIS 3+ injury. In Table 3.8, it can

be found that the test with serious liver injury had a $\dot{F}C_{max}$ value of 85.4 N/ms, more than two

orders of magnitude higher than the value reported by Kent. Although the value reported in the

study by Kent was for a swine model, the swine is a commonly used animal model and it was

expected that the magnitudes would be more similar. This difference indicates that KVC may

also depend on velocity, whether the subject has a fixed or free back, and whether the loading is

blunt or belt loading.

Scaling factors were used to normalize the data sets and the values of the normalized

variables are reported in Table 3.10. The normalized values for the lateral and oblique tests are

similar. When considering all tests, normalization of the force reduces the standard deviation

(576.1 to 450.6 N) but increases the average force significantly (4694.6 to 5739.3 N).

Normalization of the displacement from the lateral tests reduced the average displacement for

slightly from 86.9 to 83.3 mm. However, normalization of the oblique tests increased the

average value from 89.9 to 96.2 mm. This variation can be attributed to subject FBL05-O with a

normalized displacement of 115.1 mm. As for the KVC, in the lateral and oblique tests,

normalization resulted in a higher average value. The standard deviation of the KVC in the

lateral tests also increased due to normalization.

Normalization using the impulse-momentum method has been commonly used for

reducing the variation between biomechanical testing subjects. However, the method has its

limitations. First, the effective mass somewhat addresses the concerns of varying proportions of

the subjects. However, there are many variables that may affect the effective mass such as the

amount of subcutaneous fat, the interaction of the impactor face with the thorax as ribs fracture,

or the alignment of the subject with the impactor. Second, since the lateral and oblique tests

72

were considered separately, the average ratio of effective mass to the body mass was based on a very limited number of points. One outlier in this group would significantly affect the results. Adding additional subjects would change the scaling factors and hopefully reduce the variation. The normalizing factors and normalized values are reported but it is difficult to draw conclusive results from the normalized data with such a limited number of data points.

4.7 Force

The force for this test series was calculated by two methods. For the first method, the force was found by multiplying the measured ram acceleration by the mass of the ram. For the second method, the resultant force was calculated by finding the resultant of the load cell forces in the X, Y, and Z-directions and adding the inertial force in the y-direction, the primary direction of loading.

Similar trends were seen in all data sets for force so as an example, the two methods of calculating force are plotted in Figure 4.5 for test FBL03-L. The force from the ram accelerometer initially shows a negative peak as the ram begins to accelerate prior to contact with the subject. The load cell measurements do not show this because the measurements are inertially compensated. At time zero, the ram contacts the subject and both methods of force calculation show a similar force. Around 0.040 seconds, both forces show a slight increase in the force as the rate of deceleration is increased. The increase in rate of deceleration occurs because the ram impacts padding as it reaches its maximum extension to prevent the ram from bottoming out. The magnitude of the force calculated from the accelerometer is higher than the load cell force because the change in force occurs at the back end of the ram where the protection padding is located. The load cell only directly measures the force at the front end of the ram that interacts with the subject. The load cell does indirectly measure the force caused

by the change in the acceleration but this force should be removed with the addition of the
inertial force to the load cell measured forces.
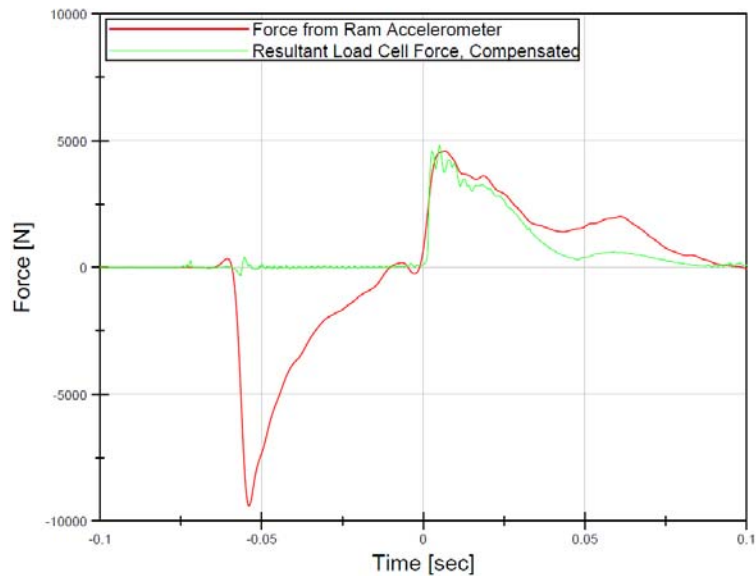
Figure 4.5: Applied Force vs. Time for FBL03-L

For this testing, the time period of interest is from time zero to the point of maximum
compression. The maximum compression occurs between 0.02345 s and 0.0254 s in this test
series, well before the ram has reached its maximum extension so the difference in the force
magnitude is not a major concern. There is some discrepancy with the forces before the time of
maximum compression. The variance could be due to the fact that the accelerometer is not
located in line with the load cell or due to noise from the load cell or accelerometer signals. For
this research, the force from the accelerometer signals was used to measure the applied force
because this is a more common practice in crash test analysis since it is not always possible to
locate a load cell at the position of impact.

4.8 Chestband Analysis

The chestband provides a measure of time history of the compression of the thorax. Figure 3.10 through Figure 3.14 show how the chestband moves through time. It should be kept in mind when looking at these figures that the spine was held fixed to plot the data. The plots do not show the movement or rotation of the thorax. The average compressions for the lateral and oblique tests were similar; for the lateral tests the average compression was 0.29 while the average compression for the oblique tests was 0.30. In all the tests, the spine and sternum move apart upon impact as the thorax is compressed. Most of the compression occurs between 0 and 0.10 seconds. Minimal additional compression is seen between 0.015 s and the maximum compression, as seen by similar chestband curves for times after 0.015 s. For the lateral tests, most of the displacement occurs on the right half of the thorax but some displacement occurs as the left side comes in toward the gage at the spine. One limitation of the chestband is that it was not fixed to the skin so there may be compression trends that are not captured by the data. The chestband would have difficulty indentifying concavities in the thorax and would tend to simply form a straight line between the two gauges.

4.9 Force and Displacement Time Histories

The time history of the non-normalized and normalized force is shown in Figure 3.15 and Figure 3.16.   It can be seen that normalization increases the variability in the timing of the peaks and changes the rate of the force increase. There is an especially noticeable effect for the female subjects, Test FBL02-L and Test FBL05-O, where the time factor significantly changes the timing of the loading and unloading. Figure 3.17 and Figure 3.18 show the displacement-time histories with similar trends for the female subject FBL05-O for the timing. There is no compression data for the other female subject, FBL02-L. The peak magnitude for the

75

displacement of FBL05-O was the second highest measured displacement of all the subjects

(92.3 mm) and the subject's chest breadth was not significantly larger than the other subjects.

This resulted in a high compression value for this subject which may be explained by more

subcutaneous tissue on the female subject which would have been compressed during impact.

4.10 Force-Displacement and Force-Compression

Figure 3.19 and Figure 3.20 show the force-displacement and force-compression plots.

The initial loading reveals a large increase in force with minimal compression or displacement.

This is a result of the loading of the thorax prior to the chestband response beginning. When

considering the normalized force-compression curves, the lateral and oblique results were quite

similar in terms of the maximum compression and the peak force.

This result disagrees with the results from Shaw et al. (2006) which showed distinct

responses of the thorax to lateral and oblique impacts. However, there are differences between

the current setup and the setup used by Shaw et al.; the current impacts are a higher velocity

and are more inferior on the subject. Since the current study is impacting at a higher velocity,

the visco-elasticity of the thorax may cause the reaction of the thorax to be more similar

whether impacting laterally or obliquely than in the work by Shaw. Furthermore, impacting

more inferiorly means that the impactor interacts with ribs that are all connected to the

sternum through one costal cartilage connection. This means the force applied to the thorax at

that connection may be similar for lateral and oblique tests.   These reasons may account for the

current test showing similar responses for lateral and oblique impacts while Shaw et al. found

the response for the lateral and oblique impacts to be different.

4.11 Limitations

In this test series, the bottom edge of the plate was aligned with rib eleven at the mid-axillary line on the right side of the subject. This location was selected in order to try to maximize the loading of the liver by the plate. However, there was significant variation in how the plate interacted with the liver, as demonstrated in Figure 4.4. Future testing will attempt to identify the exact liver height when aligning the impact by use of the CT images or small incisions through the diaphragm to both place liver tissue sensors and to locate the liver.

It is difficult to determine the effectiveness of the pressurization. It was not possible to measure the initial pressure value relative to the ambient air for the pressure sensors since the sensors were zeroed while already in the subject's vasculature. The sensors may or may not have been in blood already in the subject's body. Following pressurization with the saline, the change from the initial pressure was known but there was not a method to ensure the abdominal vasculature had reached physiological pressure. One solution to this is to attach tubing to the subject's inferior instrumentation sites and ensure the height of the fluid column at the output would provide the correct pressure to the subject's vasculature. This would ensure consistent pressurization for each subject and provide an understanding of the pressure prior to impact. Pressurization of the liver is important in order to produce realistic injury patterns to the liver (Mays, 1966). Additionally, the pressure results showed some dependence on location relative to the impactor so consistent placement of the sensors would improve the testing.

Another limitation of the current study is the study included a limited number of data points.   It is difficult to achieve statistically significant results with only six tests. Additionally, all

the tests were at the same impact velocity and a change in velocity may change the ability of various criteria to predict abdominal injury.

It is hoped that future work will be done to continue studying abdominal injury with the correct boundary conditions provided by full body PMHS testing but improving on the impactor alignment, sensor placement, and pressurization methods.

Chapter 5: Conclusions

This test series used full body PMHS with re-pressurized abdominal vasculature to study abdominal injuries. A total of four lateral and two oblique tests were performed. The following conclusions summarize the work:

1. The tests series successfully produced injuries similar to those documented in the CIREN trauma database, including one AIS 4, burst injury to the liver in test FBL03-L.

2. P_{max} and $\dot{P}_{max}$ were shown to be correlated to location of the pressure sensors. In particular, a strong correlation was found between the resultant of the distances from the center of the impact point to the instrumentation in both the direction of impact and the superior-inferior direction.

3. Injury risk curves were created using binary logistic regressions. When considering the venous pressure sensors, the strongest predictor of serious abdominal injury (AIS 3+) was $\dot{P}_{max}$ (p<0.001, gamma=1.00). A value of $\dot{P}_{max}$ of 32.1 kPa/ms corresponds to a 50% risk of AIS 3+ injury.

4. $P_{max}\dot{P}_{max}$ and $[\dot{P}*P]_{max}$ were also shown to be good predictors of AIS 3+ injury (p=0.007, gamma=0.91 and p=0.017, gamma=0.77) according to a binary logistic regression injury risk model. Values of $P_{max}\dot{P}_{max}$ and $[\dot{P}*P]_{max}$ of 2366 and 1209 kPa^2/ms, respectively, correspond to a 50% risk of AIS 3+ injury.

5. KVC and $\dot{P}$ were shown to be linearly related (R^2 adjusted=0.60, p<0.001) as they both are measurements of the directness of the loading and the rate of the loading of the abdomen.

6. For the test with serious injury, the highest values of VC_{max} and $\dot{F}C_{max}$ were obtained with values of 1.72 m/s and 85.43 N/ms, respectively.

7. Impulse-momentum normalization did not reduce the subject variability in the displacement measured by the chestband due to impact. However, some reduction in the variability of the peak force was achieved through normalization.

The broader impact of these results is that development of abdominal inserts for ATDs should consider the results found relating injury to the directness of loading. Using a homogenous abdominal insert without mobility would not allow the directness of the loading to be measured since the insert would not be able to move out of the way in response to loading. A heterogeneous abdomen with fluid filled vessels that have mobility within the abdomen may not be practical due to limitations in robustness for car crash testing. However, the results from this work could be used in finite element testing where accurate models of liver tissue and vasculature would allow for the rate of pressure change to be calculated.

REFERENCES

Bondy, N. "Abdominal Injuries in the National Crash Severity Study." In *National Center for Statistics and Analysis Collected Technical Studies*, 59-80. Washington, D.C.: National Highway Traffic Safety Administration, 1980.

Cavanaugh, J. M., Y. Huang, Y. Zhu, and A. I. King. "Regional Tolerance of the Shoulder, Thorax, Abdomen and Pelvis to Padding in Side Impact." *S.A.E. technical paper no. 930435* 102, no. 6 (1993).

Cavanaugh, J. M., A. I. King, S. J. Goldberg, and G. W. Nyquist. "Lower Abdominal Tolerance and Response." *Stapp Car Crash Journal* 30 (1986): 41-63.

Elhagediab, A. M., and S. W. Rouhana. "Patterns of Abdominal Injury in Frontal Automotive Crashes." Paper presented at the International Technical Conference on Experimental Safety Vehicles, Washington, D.C. 1998.

Eppinger, R. H., J. H. Marcus, and R. M. Morgan. "Side Impact Data Analysis." Paper presented at the International Technical Conference on Experiemtnal Safety of Vehicles, Washington, D.C. 1984.

Guyton, A. C.. *Textbook of Medical Physiology*. Tokyo: Igaku Shoin, 1976.

Horsch, J. D., D. V. Andrzejak, D. C. Viano, and I. V. Lau. "Mechanism of Abdominal Injury by Steering Wheel Loading." *Stapp Car Crash Journal* 29 (1985): 69-78.

Kent, R., S. Stacey, M. Kindig, W. Woods, J. Evans, S. W. Rouhana, K. Higuchi, H. Tanji, S. St Lawrence, and K. B. Arbogast. "Biomechanical Response of the Pediatric Abdomen, Part 2: Injuries and Their Correlation with Engineering Parameters." *Stapp Car Crash Journal* 52 (2008): 135-66.

Lau, V. K., and D. C. Viano. "An Experimental Study on Hepatic Injury from Belt-Restraint Loading." *Aviation, Space, and Environmental Medicine* 52, no. 10 (1981): 611-17.

Lau, V. K., and D. C. Viano. "Influence of Impact Velocity on the Severity of Nonpenetrating Hepatic Injury." *The Journal of Trauma* 21, no. 2 (1981): 115-23.

Lee, J. B., and K.H. Yang. "Abdominal Injury Patterns in Motor Vehicle Accidents: A Survey of the Nass Database from 1993 to 1997." *Traffic Injury Prevention* 3, no. 3 (2002): 241-46.

Lee, R. B., S. M. Bass, J. A. Morris, Jr., and E. J. MacKenzie. "Three or More Rib Fractures as an Indicator for Transfer to a Level I Trauma Center: A Population-Based Study." *The Journal of Trauma* 30, no. 6 (1990): 689-94.

Mays, E. T. "Bursting Injuries of the Liver. A Complex Surgical Challenge." *Archives of surgery* 93, no. 1 (1966): 92-106.

McElhaney, J. H., R. L. Stalnaker, Verne L. Roberts, Richard G. Snyder, and Institute University of Michigan. Highway Safety Research. "Door Crashworthiness Criteria." *Stapp Car Crash Journal* 15 (1972): 489-517.

Melvin, J., R. L. Stalnaker, V. L. Roberts, and M. L. Trollope. "Impact Injury Mechanisms in Abdominal Organs." *Stapp Car Crash Journal* 17 (1973): 115-26.

Mertz, H. J. "A Procedure for Normalizing Impact Response Data." *S.A.E. technical paper no. 840884* 102, no. 2 (1984): 554.

Miller, M. A. "The Biomechanical Response of the Lower Abdomen to Belt Restraint Loading." *The Journal of Trauma* 29, no. 11 (1989): 1571-84.

Netter Presenter Human Anatomy Collection. (2003) Icon Learning Systems, Teterboro, NJ.

Nusholtz, G. S. "Thoraco-Abdominal Response and Injury." *Stapp Car Crash Journal* 24 (1980): 187-228.

"Obesity: Preventing and Managing the Global Epidemic." *World Health Organization technical report* 894 (2000): 1-253.

Pintar, F. A., N. Yoganandan, M. H. Hines, M. R. Maltese, J. McFadden, R. Saul, R. Eppinger, N. Khaewpong, and M. Kleinberger. "Chestband Analysis of Human Tolerance to Side Impact." *Stapp Car Crash Journal* 41 (1997): 63-74.

Prasad, P., and R. P. Daniel. "A Biomechanical Analysis of Head, Neck, and Torso Injuries to Child Surrogates Due to Sudden Torso Acceleration." *Stapp Car Crash Journal* 28 (1984): 25-40.

Ricci, L.. "NCSS Statistics : Passenger Cars." edited by UM-HSRI report 80-36: National Highway Traffic Safety Administration, 1980.

Rouhana, S. W., and M. E. Foster. "Lateral Impact - an Analysis of the Statistics in the NCSS." *Stapp Car Crash Journal* 29 (1985): 79-98.

Rouhana, S. W., I. V. Lau, and S. A. Ridella. "Influence of Velocity and Forced Compression on the Severity of Abdominal Injury in Blunt, Nonpenetrating Lateral Impact." *The Journal of Trauma* 25, no. 6 (1985): 490-500.

Rouhana, S. W., D. C. Viano, and S. A. Ridella. "The Effect of Limiting Impact Force on Abdominal Injury: A Preliminary Study." *Stapp Car Crash Journal* 30 (1986): 65-79.

Rutledge, R., C. Baker, P. Cunningham, T. Clancy, J. Moylan, W. Meredith, D. Oller, M. Thomason, "The Spectrum of Abdominal Injuries Associated with the Use of Seat Belts." *The Journal of Trauma* 31, no. 6 (1991): 820-26.

Shaw, J. M., R. G. Herriott, J. D. McFadden, B. R. Donnelly, and J. H. th Bolte. "Oblique and Lateral Impact Response of the Pmhs Thorax." *Stapp Car Crash Journal* 50 (2006): 147-67.

Shweiki, E., J. Klena, G. C. Wood, and M. Indeck. "Assessing the True Risk of Abdominal Solid Organ Injury in Hospitalized Rib Fracture Patients." *The Journal of Trauma* 50, no. 4 (2001): 684-8.

Sparks, J. L., J. H. Bolte, R. B. Dupaix, K. H. Jones, S. M. Steinberg, R. G. Herriott, J. A. Stammen, and B. R. Donnelly. "Using Pressure to Predict Liver Injury Risk from Blunt Impact." *Stapp Car Crash Journal* 51 (2007): 401-32.

Stalnaker, R. L., Verne L. Roberts, and James McElhaney. "Side Impact Tolerance to Blunt Trauma." *Stapp Car Crash Journal* 17 (1973): 377-408.

Talantikite, Y., C. Tarriere, J. Y. Le Coz, and F. Brun-Cassan. "Abdominal Injury Protection in Side Impact Injury - Injury Mechanisms and Protection Criteria." Paper presented at the International IRCOBI Conference Proceedings 1993.

Trollope, M. L., R. L. Stalnaker, J. H. McElhaney, and C. F. Frey. "The Mechanism of Injury in Blunt Abdominal Trauma." *The Journal of Trauma* 13, no. 11 (1973): 962-70.

Viano, D. C., and I. V. Lau. "Thoracic Impact: A Viscous Tolerance Criterion." Paper presented at the International Technical Conference on Experimental Safety of Vehicles, Washington, D.C. 1986.

Viano, D. C., I. V. Lau, C. Asbury, A. I. King, and P. Begeman. "Biomechanics of the Human Chest, Abdomen, and Pelvis in Lateral Impact." *Accident; analysis and prevention* 21, no. 6 (1989): 553-74.

Viano, D.C., and V.K. Lau. "Role of Impact Velocity and Chest Compression in Thoracic Injury." *Aviation, space, and environmental medicine* 54, no. 1 (1983): 16-21.

Walfisch, G., R. L. Stalnaker, A. Patel, C. Got, F. Guillon, J. P. Rosey, C. Tarriere, and A. Fayon. "Designing of a Dummy's Abdomen for Detecting Injuries in Side Impact Collisions." Paper presented at the International IRCOBI Conference Proceedings 1980.

Williams, R. D., and F. T. Sargent. "The Mechanism of Intestinal Injury in Trauma." *The Journal of Trauma* 3 (1963): 288-94.

Yoganandan, N., F. A. Pintar, T.A. Gennarelli, and M. R. Maltese. "Patterns of Abdominal Injuries in Frontal and Side Impacts." Paper presented at the Association for the Advancement of Automotive Medicine 2000.

APPENDIX A

Complete anthropometry

Subject Anthropometry

	FBL01-L	FBL02-L	FBL03-L	FBL04-L	FBL05-O	FBL06-O
Gender	M	F	M	M	F	M
Age	68	80	88	91	53	79
Mass (kg)	66.7	59.0	72.6	63.5	54	81.6
Stature (cm)	176	154	188	179	164	179
Shoulder Height (cm)	149	138	163	157	140	154
Chest Breadth (cm)	27	31	27	27.3	30	31
Waist Breadth (cm)	26	33	30	30	30	35
Seated Height (cm)	94	87	96	97	92	99
Chest Circumference (cm)	90	94	93	90	87	98
Waist Circumference (cm)	84	91	88	90	86	94
Chest Depth (cm)	20	19	19	19	17	23
Waist Depth (cm)	18	17	14	21	15	22

APPENDIX B

Explanation of Transformation to Laboratory Coordinate System

The rotations about each axis can be described by transformation matrices where the rotation about the z-axis is given by the angle ψ, the rotation about the x'-axis is θ, and the rotation about the z'-axis is σ. This is also referred to as 3-1-3 sequence of rotation.

$$D = \begin{bmatrix} \cos(\varphi) & -\sin(\varphi) & 0 \\ \sin(\varphi) & \cos(\varphi) & 0 \\ 0 & 0 & 1 \end{bmatrix}$$

[B.1]

$$C = \begin{bmatrix} 1 & 0 & 0 \\ 0 & \cos(\theta) & -\sin(\theta) \\ 0 & \sin(\theta) & \cos(\theta) \end{bmatrix}$$

[B.2]

$$B = \begin{bmatrix} \cos(\sigma) & -\sin(\sigma) & 0 \\ \sin(\sigma) & \cos(\sigma) & 0 \\ 0 & 0 & 1 \end{bmatrix}$$

[B.3]

These can be combined to give the complete transformation matrix A, defined as A=DCB.

$$A = \begin{bmatrix} \cos(\varphi)\cos(\sigma) - \sin(\varphi)\cos(\theta)\sin(\sigma) & -\cos(\varphi)\sin(\sigma) - \sin(\varphi)\cos(\theta)\cos(\sigma) & \sin(\varphi)\sin(\theta) \\ \sin(\varphi)\cos(\sigma) + \cos(\varphi)\cos(\theta)\sin(\sigma) & -\sin(\varphi)\sin(\sigma) + \cos(\varphi)\cos(\theta)\cos(\sigma) & -\cos(\varphi)\sin(\theta) \\ \sin(\theta)\sin(\sigma) & \sin(\theta)\cos(\sigma) & \cos(\theta) \end{bmatrix}$$

[B.4]

The initial transformation matrix can also be expressed in terms of the global coordinate vectors (x, y, and z) and the initial block coordinates (i, j, k).

$$A = \begin{bmatrix} \vec{x} \\ \vec{y} \\ \vec{z} \end{bmatrix} \times \begin{bmatrix} \vec{i} & \vec{j} & \vec{k} \end{bmatrix} = \begin{bmatrix} x \cdot i & x \cdot j & x \cdot k \\ y \cdot i & y \cdot j & y \cdot k \\ z \cdot i & z \cdot j & z \cdot k \end{bmatrix}$$

[B.5]

Knowing the initial transformation matrix allows us to solve for the initial Euler angles by setting terms equal:

$$A = \begin{bmatrix} x \cdot i & x \cdot j & x \cdot k \\ y \cdot i & y \cdot j & y \cdot k \\ z \cdot i & z \cdot j & z \cdot k \end{bmatrix} =$$

$$\begin{bmatrix} \cos(\varphi)\cos(\sigma) - \sin(\varphi)\cos(\theta)\sin(\sigma) & -\cos(\varphi)\sin(\sigma) - \sin(\varphi)\cos(\theta)\cos(\sigma) & \sin(\varphi)\sin(\theta) \\ \sin(\varphi)\cos(\sigma) + \cos(\varphi)\cos(\theta)\sin(\sigma) & -\sin(\varphi)\sin(\sigma) + \cos(\varphi)\cos(\theta)\cos(\sigma) & -\cos(\varphi)\sin(\theta) \\ \sin(\theta)\sin(\sigma) & \sin(\theta)\cos(\sigma) & \cos(\theta) \end{bmatrix}$$

[B.6]

Caution must be used when taking the inverse of the trigonometric functions to ensure that the value from the proper quadrant is selected. This can be verified by plugging in values for both matrices and ensuring that both sides of the equation provide the same matrix. The relationship between the angular velocity with respect to the body fixed coordinate system is related to the angular velocity of the Euler angles as follows:

$$\begin{bmatrix} \omega_x' \\ \omega_y' \\ \omega_z' \end{bmatrix} = \begin{bmatrix} \sin(\theta)\sin(\sigma) & \cos(\sigma) & 0 \\ \sin(\theta)\cos(\sigma) & -\sin(\sigma) & 0 \\ \cos(\theta) & 0 & 1 \end{bmatrix} \begin{bmatrix} \dot{\varphi} \\ \dot{\theta} \\ \dot{\sigma} \end{bmatrix}$$

[B.7]

The angular rates of the body-fixed coordinate system (ω_x, ω_y, ω_z) are measured by the ARS. In order to determine the angular velocity of the Euler angles, the inverse of the matrix is multiplied by the angular rates.

$$\begin{bmatrix} \dot{\varphi} \\ \dot{\theta} \\ \dot{\sigma} \end{bmatrix} = \begin{bmatrix} \sin(\theta)\sin(\sigma) & \cos(\sigma) & 0 \\ \sin(\theta)\cos(\sigma) & -\sin(\sigma) & 0 \\ \cos(\theta) & 0 & 1 \end{bmatrix}^{-1} \begin{bmatrix} \omega_x' \\ \omega_y' \\ \omega_z' \end{bmatrix}$$

[B.8]

The initial Euler angles were determined previously using Equation B.6. Knowing the initial angle allows us to calculate the time history of the angles with respect to the laboratory coordinate frame. The second Euler angle can be calculated as follows:

$$\varphi_2 = \varphi_1 + \dot{\varphi}_1 \times \Delta t$$
$$\theta_2 = \theta_1 + \dot{\theta}_1 \times \Delta t$$
$$\sigma_2 = \sigma_1 + \dot{\sigma}_1 \times \Delta t$$

[B.9]

These new angles can be plugged into Equation B.8 and used to calculate new values $\dot{\varphi}$,

$\dot{\theta}$, and $\dot{\sigma}$. Subsequent angles can be found as follows:

$$\varphi_{i+1} = \varphi_i + \frac{1}{2}(\dot{\varphi}_i + \dot{\varphi}_{i+1}) \times \Delta t$$
$$\theta_{i+1} = \theta_i + \frac{1}{2}(\dot{\theta}_i + \dot{\theta}_{i+1}) \times \Delta t$$
$$\sigma_{i+1} = \sigma_i + \frac{1}{2}(\dot{\sigma}_i + \dot{\sigma}_{i+1}) \times \Delta t$$

[B.10]

This iterative process will give a time history of the Euler angles with respect to the

laboratory coordinate frame. This allows for the time history of the transformation matrix time

history to be calculated and used to transform the time history of the accelerometers and

angular rate sensors. Double integration of the accelerometers provides the displacement in

each direction of the laboratory coordinate system. Integration of the angular rate sensors

provides the angular displacement. The code for completing the transformations is provided.

CONTROL FILE

```
%  This matlab code is to transform data from accelerometers and angular rate sensors to the
Lab Coordinate System
%  H. Gustafson
%  June, 2009

clear all
close all

%---------------Load Data-------------------
POINTLIST=xlsread ('0829FBL70R01_input_F', 'Faro');                          %in units of mm
Accel=xlsread ('0829FBL70R01_input_F', 'Accels');              %in units of G
DTS=xlsread ('0829FBL70R01_input_F', 'DTS');                    %in units of deg/s
DTS= DTS.*pi/180;                                               %convert to units of rad/s
len=length(Accel);
%---------------Determine Global Coordinate System(BCS)--------------
%  Uses Posterior Superior Iliac Spines and Anterior Superior Iliac Spines to define desired
coordinate system
RTPSIS=POINTLIST(1,1:3);
LTPSIS=POINTLIST(2,1:3);
RTASIS=POINTLIST(3,1:3);
LTASIS=POINTLIST(4,1:3);
MIDPSIS=(RTPSIS+LTPSIS)./2;
MIDASIS=(RTASIS+LTASIS)./2;
%tip-tail
Ytemp=RTPSIS-LTPSIS;
Xtemp=MIDASIS-MIDPSIS;
Ztemp=cross(Xtemp, Ytemp);
Xtemp=cross(Ytemp,Ztemp);
xaxis=Xtemp/norm(Xtemp);
yaxis=Ytemp/norm(Ytemp);
zaxis=Ztemp/norm(Ztemp);

%----------Determine initial angles of each block------------------
[phi_st, theta_st, sigma_st]= Func_Euler(POINTLIST(5:7, 1:3), xaxis, yaxis, zaxis);
[phi_thr1, theta_thr1, sigma_thr1]= Func_Euler(POINTLIST(8:10, 1:3), xaxis, yaxis, zaxis);
[phi_thr8, theta_thr8, sigma_thr8]= Func_Euler(POINTLIST(11:13, 1:3), xaxis, yaxis, zaxis);
[phi_thr12, theta_thr12, sigma_thr12]= Func_Euler(POINTLIST(14:16, 1:3), xaxis, yaxis, zaxis);

%---------Determine the angle time history for each block and the transformation--------------------
-
[accel_st, dts_st, angle_st, disp_st, ang_st]= Func_trans(phi_st, theta_st, sigma_st, Accel(:,1:3),
DTS(:,1:3));
[accel_thr1, dts_thr1, angle_thr1, disp_thr1, ang_thr1]= Func_trans(phi_thr1, theta_thr1,
sigma_thr1, Accel(:,4:6), DTS(:,4:6));
```

[accel_thr8, dts_thr8, angle_thr8, disp_thr8, ang_thr8]= Func_trans(phi_thr8, theta_thr8, sigma_thr8, Accel(:,7:9), DTS(:,7:9));
[accel_thr12, dts_thr12, angle_thr12, disp_thr12, ang_thr12]= Func_trans(phi_thr12, theta_thr12, sigma_thr12, Accel(:,10:12), DTS(:,10:12));
%---------Defines the headers of the output excel files----------------
hd1={'STRNX_acc', 'STRNY_acc', 'STRNZ_acc', 'T1X_acc', 'T1Y_acc', 'T1Z_acc', 'T8X_acc', 'T8Y_acc', 'T8Z_acc', 'T12X_acc', 'T12Y_acc', 'T12Z_acc' ; 'G' 'G' 'G' 'G' 'G' 'G' 'G' 'G' 'G' 'G' 'G' 'G'};
hd2={'STRNX_ars', 'STRNY_ars', 'STRNZ_ars', 'T1X_ars', 'T1Y_ars', 'T1Z_ars', 'T8X_ars', 'T8Y_ars', 'T8Z_ars', 'T12X_ars', 'T12Y_ars', 'T12Z_ars' ; 'deg/s' 'deg/s' 'deg/s' 'deg/s' 'deg/s' 'deg/s' 'deg/s' 'deg/s' 'deg/s' 'deg/s' 'deg/s' 'deg/s'};
hd3={'STRNX_disp', 'STRNY_disp', 'STRNZ_disp', 'T1X_disp', 'T1Y_disp', 'T1Z_disp', 'T8X_disp', 'T8Y_disp', 'T8Z_disp', 'T12X_disp', 'T12Y_disp', 'T12Z_disp' ; 'mm' 'mm' 'mm' 'mm' 'mm' 'mm' 'mm' 'mm' 'mm' 'mm' 'mm' 'mm'};
hd4={'STRNX_angdisp', 'STRNY_angdisp', 'STRNZ_angdisp', 'T1X_angdisp', 'T1Y_angdisp', 'T1Z_angdisp', 'T8X_angdisp', 'T8Y_angdisp', 'T8Z_angdisp', 'T12X_angdisp', 'T12Y_angdisp', 'T12Z_angdisp' ; 'deg' 'deg' 'deg' 'deg' 'deg' 'deg' 'deg' 'deg' 'deg' 'deg' 'deg' 'deg'};
% Writes the headers to the excel file
xlswrite('0829FBL70R01_output_F.xls', hd1, 'Acceleration', 'A1');
xlswrite('0829FBL70R01_output_F.xls', hd2, 'DTS', 'A1');
xlswrite('0829FBL70R01_output_F.xls', hd3, 'Displacement', 'A1');
xlswrite('0829FBL70R01_output_F.xls', hd4, 'Angular Displacement', 'A1');

% Writes the data to the excel file
xlswrite('0829FBL70R01_output_F.xls', [accel_st, accel_thr1, accel_thr8, accel_thr12], 'Acceleration', 'A3');
xlswrite('0829FBL70R01_output_F.xls', [dts_st, dts_thr1, dts_thr8, dts_thr12], 'DTS', 'A3');
xlswrite('0829FBL70R01_output_F.xls', [disp_st, disp_thr1, disp_thr8, disp_thr12], 'Displacement', 'A3');
xlswrite('0829FBL70R01_output_F.xls', [ang_st, ang_thr1, ang_thr8, ang_thr12], 'Angular Displacement', 'A3');

EULER ANGLE FUNCTION
% Given the faro points, determines the initial Euler angles of the block
function [Phi_0, Theta_0, Sigma_0] = Func_Euler(block_pts, xaxis, yaxis, zaxis)
a=block_pts(2,:)-block_pts(1,:);
k=a/norm(a);
b=block_pts(2,:)-block_pts(3,:);
j=b/norm(b);
i=cross(k,j);
i=i/norm(i);
j=cross(i,k);
j=j/norm(j);

% Defines transformation matrix based on block vectors (i, j, k) and global coordinates (x, y, z)
matrix=zeros(3,3);

91

```
matrix(1,1)=dot(i,xaxis);
matrix(1,2)=dot(j,xaxis);
matrix(1,3)=dot(k,xaxis);
matrix(2,1)=dot(i,yaxis);
matrix(2,2)=dot(j,yaxis);
matrix(2,3)=dot(k,yaxis);
matrix(3,1)=dot(i,zaxis);
matrix(3,2)=dot(j,zaxis);
matrix(3,3)=dot(k,zaxis);

Ini_A=matrix
% Determine initial Euler angle (3-1-3)
theta_1 = acos(Ini_A(3,3))
Phi_1_1_1 = atan(-Ini_A(1,3)/Ini_A(2,3))
Sigma_3_1_1 = atan(Ini_A(3,1)/Ini_A(3,2))

Phi_1_1_2 = pi+atan(-Ini_A(1,3)/Ini_A(2,3))
Sigma_3_1_2 = pi+atan(Ini_A(3,1)/Ini_A(3,2))

q1 = [0;0;0;Phi_1_1_1  ;theta_1; Sigma_3_1_1];
q2 = [0;0;0;Phi_1_1_2  ;theta_1; Sigma_3_1_1];
q3 = [0;0;0;Phi_1_1_1  ;theta_1; Sigma_3_1_2];
q4 = [0;0;0;Phi_1_1_2  ;theta_1; Sigma_3_1_2];

% Check the initial Euler angle
K1=Func_A(q1)
K2=Func_A(q2)
K3=Func_A(q3)
K4=Func_A(q4)

er=0.0001;
if (abs(Ini_A(2,1) - K1(2,1)+Ini_A(2,2)-K1(2,2)+Ini_A(2,3)-K1(2,3))<er)
    ini_euler = [Phi_1_1_1, theta_1, Sigma_3_1_1];
        else if (abs(Ini_A(2,1) - K2(2,1)+Ini_A(2,2)-K2(2,2)+Ini_A(2,3)-K2(2,3))<er)
            ini_euler = [Phi_1_1_2, theta_1, Sigma_3_1_1];
                else if (abs(Ini_A(2,1) - K3(2,1)+Ini_A(2,2)-K3(2,2)+Ini_A(2,3)-K3(2,3))<er)
                    ini_euler = [Phi_1_1_1, theta_1, Sigma_3_1_2];
                        else if (abs(Ini_A(2,1) - K4(2,1)+Ini_A(2,2)-K4(2,2)+Ini_A(2,3)-K4(2,3))<er)
                            ini_euler = [Phi_1_1_2, theta_1, Sigma_3_1_2];
                        end
                end
        end
end
Ini_Euler = ini_euler;
Phi_0=Ini_Euler(1);
Theta_0=Ini_Euler(2);
```

Sigma_0=Ini_Euler(3);

TRANSFORMATION MATRIX FUNCTION
% Given angle inputs, outputs the corresponding transformation matrix
function A=Func_A(Q)
A = zeros(3,3);
   A(1,1)=cos(Q(4))*cos(Q(6))-sin(Q(4))*cos(Q(5))*sin(Q(6));
   A(1,2)=-cos(Q(4))*sin(Q(6))-sin(Q(4))*cos(Q(5))*cos(Q(6));
   A(1,3)= sin(Q(4))*sin(Q(5));
   A(2,1)=sin(Q(4))*cos(Q(6))+cos(Q(4))*cos(Q(5))*sin(Q(6));
   A(2,2)=-sin(Q(4))*sin(Q(6))+cos(Q(4))*cos(Q(5))*cos(Q(6));
   A(2,3)=-cos(Q(4))*sin(Q(5));
   A(3,1)=sin(Q(5))*sin(Q(6));
   A(3,2)=sin(Q(5))*cos(Q(6));
   A(3,3)=cos(Q(5));

TRANSFORMATION FUNCTION
%Given the input of the initial angles as well as the accel and DTS data, it will return the
transformed accel, DTS %data, and displacement
function [accel_xyz, dts_xyz, angle_xyz, disp_xyz, ang_xyz]= Func_trans(phi_0, theta_0, sigma_0,
accel, omega)
n=length(accel);
delt=1/20000;
accel=[accel(:,1), -accel(:,2), accel(:,3)];
%---------------Initialize variables----------------
phi(1)=phi_0;
theta(1)=theta_0;
sigma(1)=sigma_0;
i=1
%--------------Define initial angular displacements----------------
B=zeros(3,3);
B(1,1)=sin(theta(i))*sin(sigma(i));
B(1,2)=cos(sigma(i));
B(1,3)=0;
B(2,1)=sin(theta(i))*cos(sigma(i));
B(2,2)=-sin(sigma(i));
B(2,3)=0;
B(3,1)=cos(theta(i));
B(3,2)=0;
B(3,3)=1;
omega_x=omega(i, 1);
omega_y=omega(i, 2);
omega_z=omega(i, 3);
ang(i,1:3)=inv(B)*[omega_x; omega_y; omega_z];
93

```
phi_dot(i)=ang(i,1);
theta_dot(i)=ang(i,2);
sigma_dot(i)=ang(i,3);
phi(2)=phi(i)+phi_dot(i)*delt;
theta(2)=theta(i)+theta_dot(i)*delt;
sigma(2)=sigma(i)+sigma_dot(i)*delt;
%-------------Define time history of phi, theta, and sigma in global coordinates----------
for i=2:n
    B=zeros(3,3);
    B(1,1)=sin(theta(i))*sin(sigma(i));
    B(1,2)=cos(sigma(i));
    B(1,3)=0;
    B(2,1)=sin(theta(i))*cos(sigma(i));
    B(2,2)=-sin(sigma(i));
    B(2,3)=0;
    B(3,1)=cos(theta(i));
    B(3,2)=0;
    B(3,3)=1;
    omega_x=omega(i, 1);
    omega_y=omega(i, 2);
    omega_z=omega(i, 3);
    ang(i,1:3)=inv(B)*[omega_x; omega_y; omega_z];
    phi_dot(i)=ang(i,1);
    theta_dot(i)=ang(i,2);
    sigma_dot(i)=ang(i,3);
    phi(i+1)=phi(i)+0.5*(phi_dot(i-1)+phi_dot(i))*delt;
    theta(i+1)=theta(i)+0.5*(theta_dot(i-1)+theta_dot(i))*delt;
    sigma(i+1)=sigma(i)+0.5*(sigma_dot(i-1)+sigma_dot(i))*delt;
end
angle_xyz=[phi', theta', sigma'];
for i=1:n
    A=zeros(3,3);
    A(1,1)=cos(phi(i))*cos(sigma(i))-sin(phi(i))*cos(theta(i))*sin(sigma(i));
    A(1,2)=-cos(phi(i))*sin(sigma(i))-sin(phi(i))*cos(theta(i))*cos(sigma(i));
    A(1,3)=sin(phi(i))*sin(theta(i));
    A(2,1)=sin(phi(i))*cos(sigma(i))+cos(phi(i))*cos(theta(i))*sin(sigma(i));
    A(2,2)=-sin(phi(i))*sin(sigma(i))+cos(phi(i))*cos(theta(i))*cos(sigma(i));
    A(2,3)=-cos(phi(i))*sin(theta(i));
    A(3,1)=sin(theta(i))*sin(sigma(i));
    A(3,2)=sin(theta(i))*cos(sigma(i));
    A(3,3)=cos(theta(i));
    accel_xyz(i, :)=A*accel(i, 1:3)';              %units of G
end
for i=1:n
    A=zeros(3,3);
    A(1,1)=cos(phi(i))*cos(sigma(i))-sin(phi(i))*cos(theta(i))*sin(sigma(i));
```

```matlab
    A(1,2)=-cos(phi(i))*sin(sigma(i))-sin(phi(i))*cos(theta(i))*cos(sigma(i));
    A(1,3)=sin(phi(i))*sin(theta(i));
    A(2,1)=sin(phi(i))*cos(sigma(i))+cos(phi(i))*cos(theta(i))*sin(sigma(i));
    A(2,2)=-sin(phi(i))*sin(sigma(i))+cos(phi(i))*cos(theta(i))*cos(sigma(i));
    A(2,3)=-cos(phi(i))*sin(theta(i));
    A(3,1)=sin(theta(i))*sin(sigma(i));
    A(3,2)=sin(theta(i))*cos(sigma(i));
    A(3,3)=cos(theta(i));
    dts_xyz(i, :)=A*omega(i, 1:3)';          %units of deg/s
end
disp_xyz=dintegrate(accel_xyz);          %units of mm
ang_xyz=180/pi*aintegrate(dts_xyz);      %units of deg
```

LINEAR DISPLACEMENT FUNCTION

```matlab
% Double integrates the accelerations to get the displacements
function disp= dintegrate(acc)
ONE=acc(:, 1)';
TWO=acc(:, 2)';
THREE=acc(:, 3)';
delt=1/20000;
DISPONE=(delt*cumtrapz(delt*cumtrapz(ONE*9.8066)))*1000;
DISPTWO=(delt*cumtrapz(delt*cumtrapz(TWO*9.8066)))*1000;
DISPTHREE=(delt*cumtrapz(delt*cumtrapz(THREE*9.8066)))*1000;
disp=[DISPONE', DISPTWO', DISPTHREE'];
```

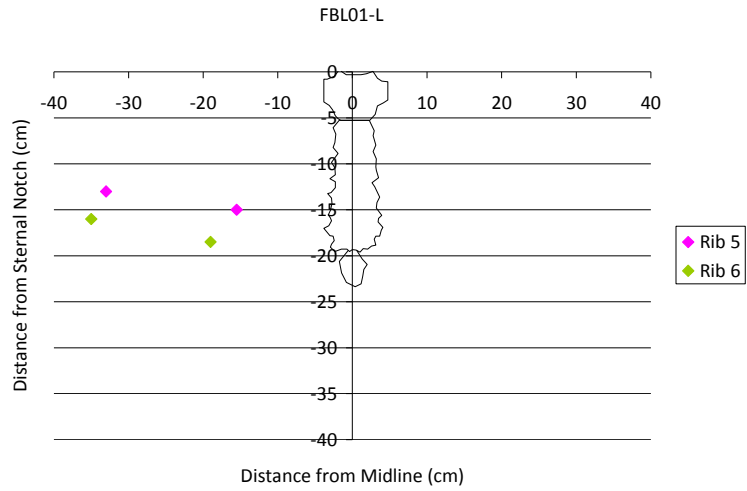**ANGULAR DISPLACEMENT FUNCTION**

```matlab
% Integrates the angular velocity to get the displacements
function angl= aintegrate(ARS)
ONE=ARS(:, 1)';
TWO=ARS(:, 2)';
THREE=ARS(:, 3)';
delt=1/20000;
DISPONE=(delt*cumtrapz(ONE));
DISPTWO=(delt*cumtrapz(TWO));
DISPTHREE=(delt*cumtrapz(THREE));
angl=[DISPONE', DISPTWO', DISPTHREE'];
```
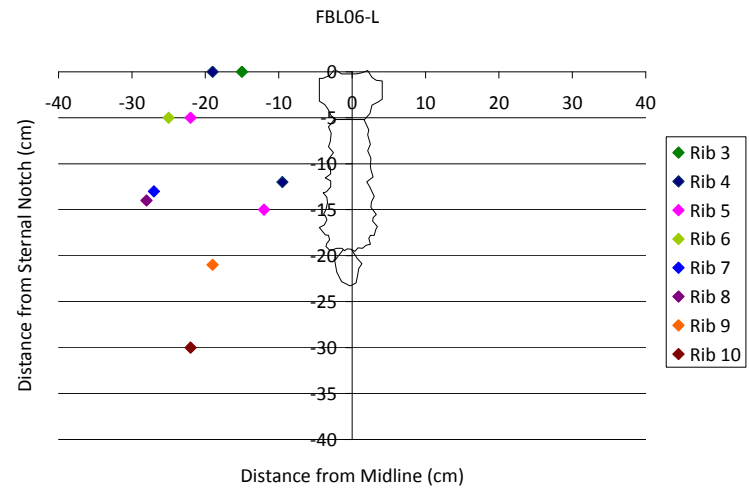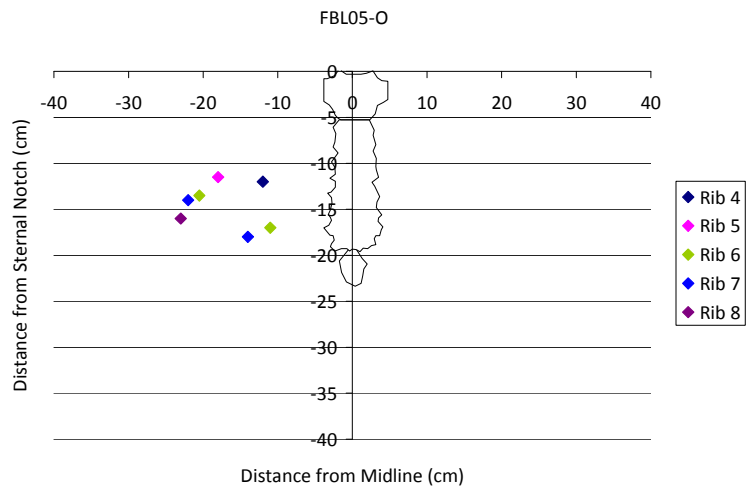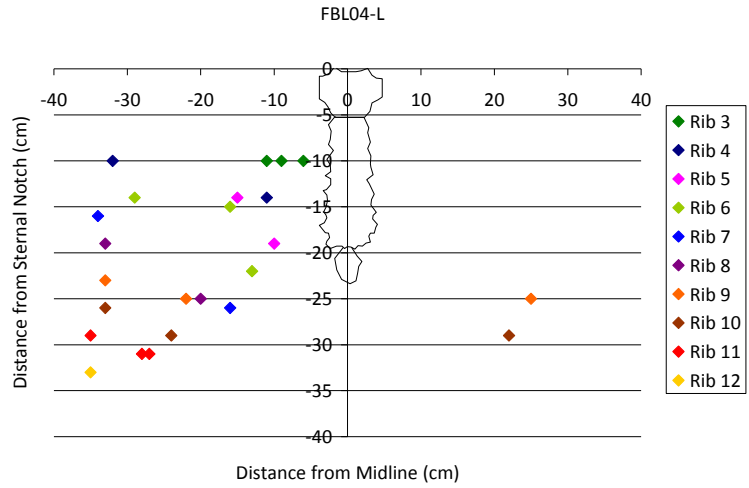
APPENDIX C

Injuries

The plots which are shown here document the locations of the rib fractures, relative to the sternum. During autopsy of the subjects, the rib fractures were located by measuring the circumferential distance around the rib cage from the sternum midline in the transverse plane and the distance from the sternal notch. As you move inferiorly down the rib cage, the circumference of the rib cage increases which is shown on the graphs as the fractures being further from the midline.

FBL01-L

Distance from Sternal Notch (cm)

Distance from Midline (cm)

Rib 5
Rib 6

FBL02-L

Distance from Sternal Notch (cm)

Distance from Midline (cm)

Rib 2
Rib 3
Rib 4
Rib 5
Rib 6
Rib 7
Rib 8
Rib 9
Rib 10
Rib 11
Rib 12

FBL03-L

Distance from Sternal Notch (cm)

Distance from Midline (cm)

Rib 6
Rib 7
Rib 8
Rib 9
Rib 10
Rib 11

98

FBL04-L

FBL05-O

FBL06-L

99
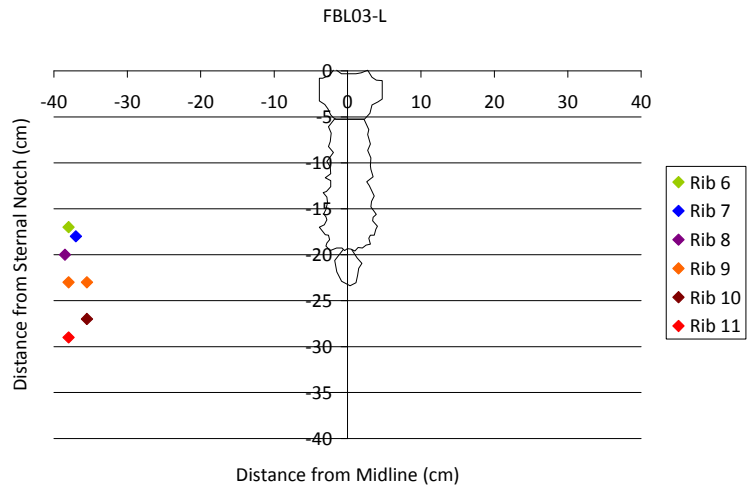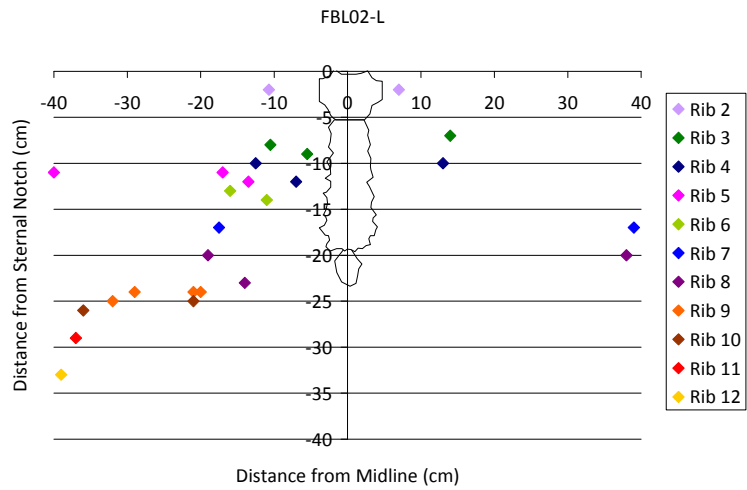
FBL01-L

Location	Description	AIS Code	AIS Level
Muscles	There was slight bruising on the right lateral aspect of the external oblique	490402.1	1-Minor
Gallbladder	Removed and biliary vessels were replaced with artificial vessels		
Liver	Adhesions to the greater omentum on entire surface, 3 cm laceration on the right, inferior aspect of the liver	541822.2	2- Moderate
Ribs	Fractures on right ribs 5 and 6	450220.2	2- Moderate

FBL02-L

Location	Description	AIS Code	AIS Level
Muscles	Blood pooling at the impact site in the external oblique muscle on the anterior side.	490402.1	1-Minor
Lungs	Right Side Pnueumothorax	441406.3	3- Serious
Liver	Slight discoloration of liver tissue at the impact site and on the left lobe.		
Stomach	Intact but air in it from pressurization with air.		
Ribs	Fractures on right rib 2 through 12, left rib 2 through 4 and 7 and 8	450266.5	5- Critical
Transverse Processes	Fractures of the transverse processes of the lumbar vertebrae, left 2 through 4 and right 1 through 4	650620.2	2- Moderate

FBL03-L

Location	Description	AIS Code	AIS Level
Muscles	Muscle bruising on serratus posterior over top of rib fractures on right side, Slight bruising on pectoralis major near distal attachment at the axilla	490402.1	1-Minor
Liver	No superficial injuries to the anterior surface of the liver Burst injury to the liver on the posterior side of the liver, primarily to the right lobe of the liver	541826.4	4- Severe
Ribs	Fractures of right ribs 6 through 12	450230.3	3- Serious

FBL04-L

Location	Description	AIS Code	AIS Level
Vasculature	The vessels near the arch of the aorta had significant amounts of plaque.		
Muscles	Pooling near T12 instrumentation		
Liver	No injury, old scar on superior aspect of liver at the axillary midline		
Ribs	Fractures of right ribs 3 through 12 and left ribs 9 and 10	450262.3	3- Serious
Transverse Processes	Fractures of the transverse processes of the lumbar vertebrae, left 2 through 4 and right 1 through 4	650620.2	2- Moderate

FBL05-O

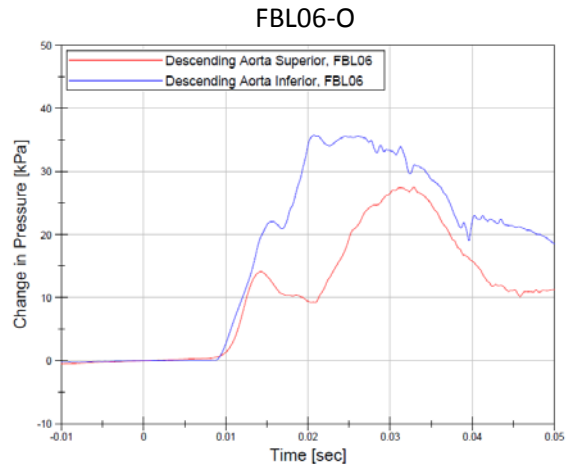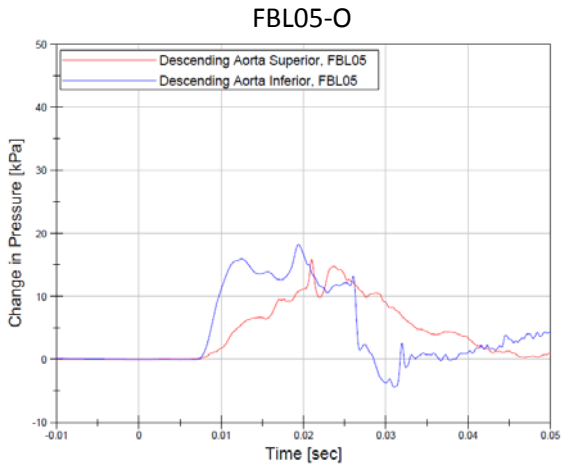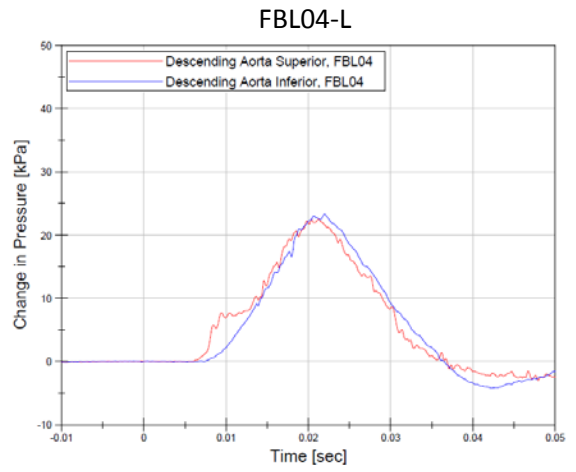| Location	Description	AIS Code	AIS Level
Liver	Laceration on anterior right lobe, 3.5 cm, Laceration on posterior right lobe, 4 cm long x 1.5 cm deep, areas of capsular damage, 4 x 4 cm and 5 x 2 cm	541820.2	2- Moderate
Ribs	Fractures of right ribs 4 through 8	450262.3	3- Serious

FBL06-O

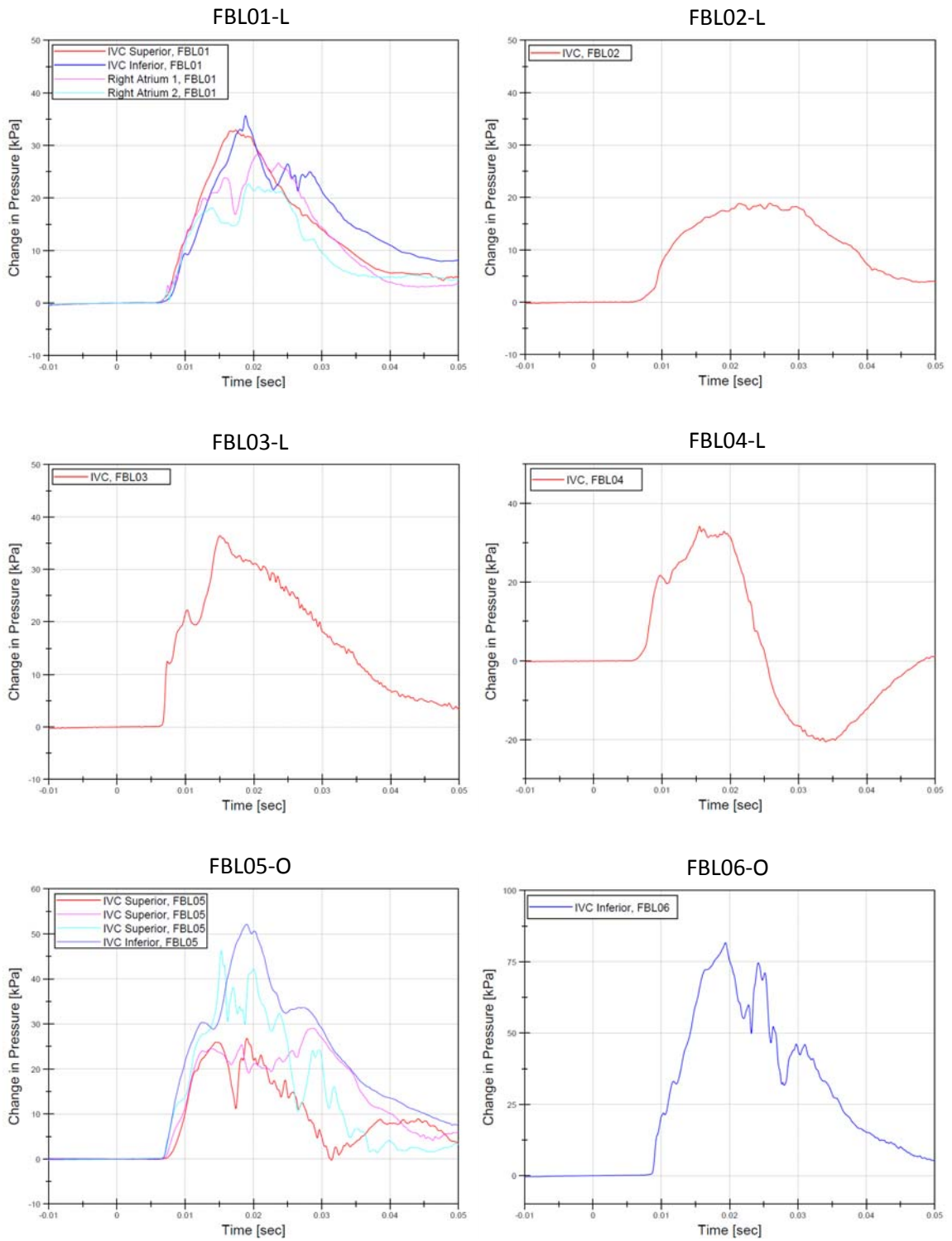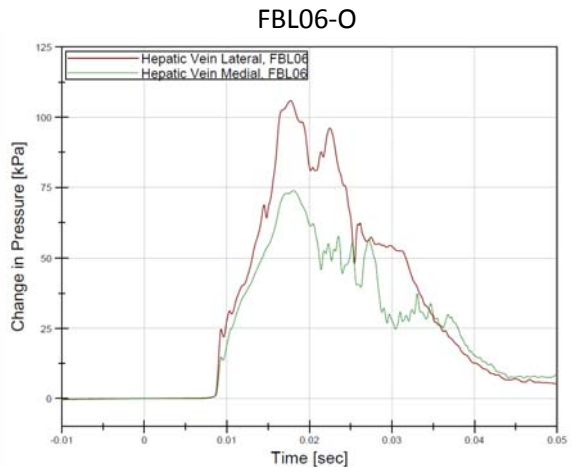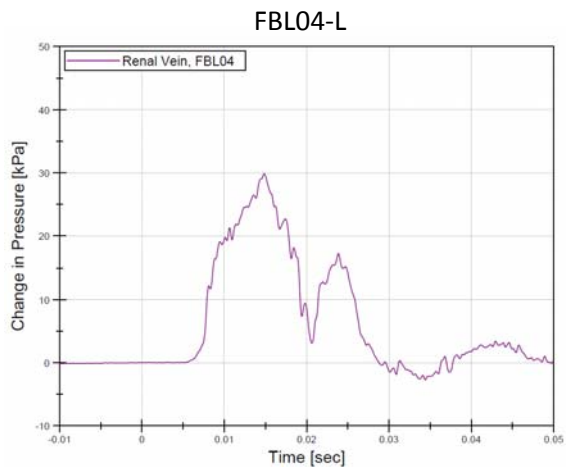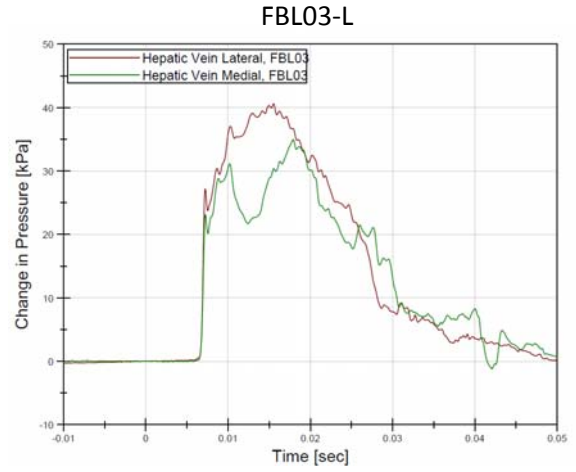| Location	Description	AIS Code	AIS Level
Liver	Three transverse lacerations across anterior surface of liver, 5 cm, 7 cm, and 8 cm Internally, right lobe tissue disruption 5 cm x 3 cm x 1 cm	541820.2, 541812.2	2- Moderate
Ribs	Fractures of right ribs 3 through 10	450262.3	3- Serious

APPENDIX D

Pressure Time Histories

Abdominal Aorta Pressure Sensors

FBL01-L

FBL02-L

FBL03-L

FBL04-L

FBL05-O

FBL06-O
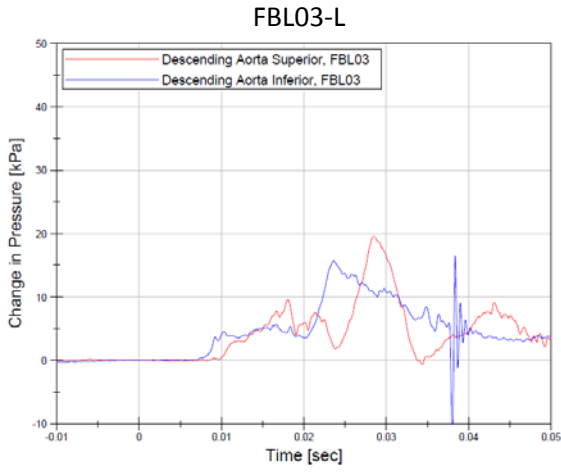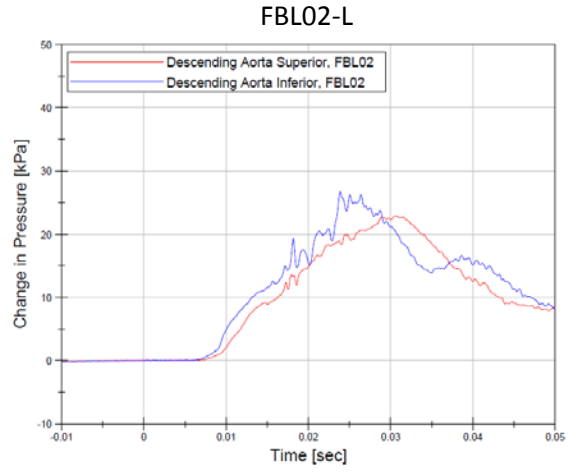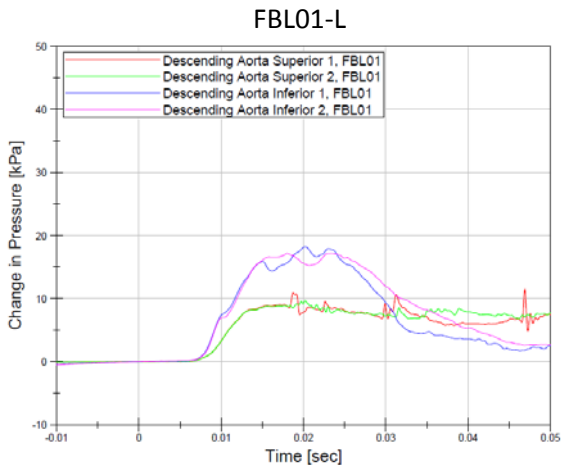
Inferior Vena Cava Pressure Sensors

FBL01-L

FBL02-L

FBL03-L

FBL04-L

FBL05-O

FBL06-O

Abdominal Organ Pressure Sensors

FBL02-L

FBL03-L

FBL04-L

FBL06-O
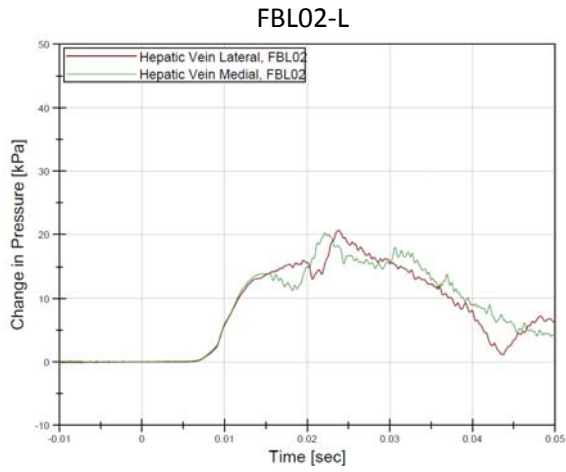
Liver Tissue Pressure Sensors

FBL05-O

FBL06-O